Loss of perilipin 2 in cultured myotubes enhances lipolysis and redirects the metabolic energy balance from glucose oxidation towards fatty acid oxidation

Yuan Z. Feng,* Jenny Lund,[1],* Yuchuan Li,[1],† Irlin K. Knabenes,* Siril S. Bakke,*
Eili T. Kase,* Yun K. Lee,§ Alan R. Kimmel,§ G. Hege Thoresen,*,** Arild Christian Rustan,*
and Knut Tomas Dalen[2],†,††

Department of Pharmaceutical Biosciences,* School of Pharmacy, Faculty of Mathematics and Natural Sciences, Department of Nutrition,† and The Norwegian Transgenic Center,†† Institute of Basic Medical Sciences, Department of Pharmacology,** Institute of Clinical Medicine, Faculty of Medicine, University of Oslo, Oslo, Norway; and Laboratory of Cellular and Developmental Biology,§ National Institute of Diabetes and Digestive and Kidney Diseases, National Institutes of Health, Bethesda, MD

ORCID ID: 0000-0002-0270-5982 (K.T.D.)

Abstract Lipid droplet (LD) coating proteins are essential for the formation and stability of intracellular LDs. Plin2 is an abundant LD coating protein in skeletal muscle, but its importance for muscle function is unclear. We show that myotubes established from $Plin2^{-/-}$ mice contain reduced content of LDs and accumulate less oleic acid (OA) in triacylglycerol (TAG) due to elevated LD hydrolysis in comparison with $Plin2^{+/+}$ myotubes. The reduced ability to store TAG in LDs in $Plin2^{-/-}$ myotubes is accompanied by a shift in energy metabolism. $Plin2^{-/-}$ myotubes are characterized by increased oxidation of OA, lower glycogen synthesis, and reduced glucose oxidation in comparison with $Plin2^{+/+}$ myotubes, perhaps reflecting competition between FAs and glucose as part of the Randle cycle. In accord with these metabolic changes, $Plin2^{-/-}$ myotubes have elevated expression of $Ppara$ and $Ppargc1a$, transcription factors that stimulate expression of genes important for FA oxidation, whereas genes involved in glucose uptake and oxidation are suppressed. Loss of $Plin2$ had no impact on insulin-stimulated Akt phosphorylation. Our results suggest that Plin2 is essential for protecting the pool of skeletal muscle LDs to avoid an uncontrolled hydrolysis of stored TAG and to balance skeletal muscle energy metabolism.—Feng, Y. Z., J. Lund, Y. Li, I. K. Knabenes, S. S. Bakke, E. T. Kase, Y. K. Lee, A. R. Kimmel, G. H. Thoresen, A. C. Rustan, and K. T. Dalen.

Energy to drive contraction of skeletal muscle fibers is obtained primarily by oxidation of glucose or FAs. Skeletal muscle cells store these two energy sources as cytosolic glycogen or triacylglycerol (TAG)-containing lipid droplets (LDs), respectively. Incorporation of glucose into glycogen and its degradation for energy utilization are relatively more understood processes than are storage and metabolism of muscular lipids. Aerobic glucose utilization occurs in the cytosol catalyzed by the glycolytic enzymes, whereas FAs are

mainly utilized through mitochondrial β-oxidation. In addition to hormonal regulation and transcription input of these two separate oxidative pathways, competitive and feedback interactions among their various substrates and products also directs glucose/FA oxidative balance and may be mechanistically important for tissue insulin sensitivity (1). Likewise, a high content of intramyocellular TAG, suggestive of increased FA availability, is well known to correlate with reduced glucose disposal and insulin resistance in some individuals (2–6), but this is not absolute. Intramyocellular TAG content in endurance-trained individuals, which can be higher than in obese insulin-resistant individuals (7), does not affect insulin sensitivity or oxidative capacity, a phenomenon described as the athlete's paradox (7–10). In addition, despite higher intramyocellular TAG levels, women are more insulin sensitive than are men (11). Therefore, new concepts have emerged to explain lipid-mediated muscular insulin resistance, which focus on abnormal lipid influx, storage, or build-up of lipid species arising from altered TAG lipolysis, rather than lipid content per se (12).

LDs in mammalian cells consist of an inner core of neutral lipids, such as TAGs, diacylglycerols (DAGs), or cholesteryl esters (CEs), surrounded by a single monolayer of phospholipids (PLs) with a protein coat (13, 14). The mechanisms for enzymatic degradation of the esterified neutral lipids in the LD core into FAs and glycerol in skeletal muscle are similar to those of many other tissues and involve active translocation of lipases to the LD surface. Thus, facilitated recruitment of proteins to the LD surface is the major mechanism regulating LD size and turnover. Adipose triglyceride lipase (ATGL) mediates the first step in TAG degradation (15), generating DAG, which is subsequently degraded by hormone-sensitive lipase (HSL) (16), followed by monoacylglycerol (MAG) cleavage by MAG lipase (17). Still, it is not understood mechanistically how lipases are actively recruited to the LD surface in muscle or how these enzymes can access the neutral lipids stored in the LD core through the protein and PL layer. Accumulating evidence suggests that perilipin (Plin) family proteins are involved [see reviews (8, 14, 18)]. As with other mammalian cell types, Plin proteins are among the most abundant LD coating proteins in skeletal muscle cells. The Plins derive from an ancient gene family that consists of five *Plin* genes in mammals, some with alternative splice variants (18–20). The *Plin* genes differ in their tissue expression and transcriptional regulation, and the encoded proteins differ in the number of residues, affinity to LDs, and stability when not bound to LDs. The fundamental understanding of Plin functions is based on the initial characterization of Plin1 in white adipose tissue. Plin1 interactions with lipases and their coactivators at the LD surface are differentially regulated by PKA phosphorylation (21) and serve as major regulatory steps controlling storage versus degradation of neutral lipids stored in the core of adipose LDs (22, 23). The other Plins are believed to regulate LD degradation in nonadipose tissues. This assumption is supported by the observations that removal of *Plin1* (22, 23), *Plin2* (24), *Plin4* (25), or *Plin5* (26) in mice results in reduced LD content in tissues where these proteins normally would be highly expressed. Overexpression of certain Plins increases the relative LD accumulation of specific neutral lipid species as opposed to others, which suggests diversity of Plin function (27).

Plin2 is an abundant LD coating protein in skeletal muscle where the majority of the LDs are covered by Plin2 (28). Interventions that increase muscle insulin sensitivity might be accompanied with an increase in Plin2 protein expression (29), suggesting that Plin2 might play a role in decreasing intramuscular lipid toxicity by promoting lipid storage. On the other hand, comparable muscular Plin2 protein content has been observed when comparing obese nondiabetic and obese diabetic subjects (30). To clarify the functional role of Plin2 in skeletal muscle, we established myoblast cultures from $Plin2^{+/+}$ and $Plin2^{-/-}$ mice, differentiated these into myotubes, and compared myocellular lipid storage and energy metabolism. We observed enhanced lipolysis, reduced levels of TAG-containing LDs, and altered lipid and glucose oxidation rates in myotubes lacking Plin2 at the LD surface. $Plin2^{-/-}$ myotubes show a shift in metabolic energy utilization toward FA oxidation, consistent with suppression of glucose oxidation within the parameters of the Randle cycle. Our results suggest that Plin2 balances energy utilization of glucose and FAs by stabilizing and packaging excess FAs in LD stores.

MATERIALS AND METHODS

Materials

DMEM (DMEM-Glutamax™, 5.5 mM glucose) with sodium pyruvate, DMEM without phenol red, Ham's F-10-Glutamax™ nutrient mixture (5.5 mM glucose), horse serum, heat-inactivated FBS, basic fibroblast growth factor, collagenase II, penicillin-streptomycin, and amphotericin B, Bodipy 493/503, Hoechst 33258, Hoechst 33342, ABI 6100 Nucleic Acid Prep-Station solutions, and Superscript III RT were from Thermo Fisher Scientific (Waltham, MA). Matrigel was purchased from BD Biosciences (Bedford, MA). Insulin (Actrapid®) was obtained from Novo Nordisk (Bagsvaerd, Denmark). BSA (essentially FA free), L-carnitine, Dulbecco's PBS (DPBS, with Mg^{2+} and Ca^{2+}), oleic acid (OA; 18:1, n-9), and glycogen were from Sigma-Aldrich (St. Louis, MO). [1-^{14}C]oleic acid (58.2 mCi/mmol) and D-[^{14}C-(U)]glucose (2.9 mCi/mmol) were from PerkinElmer NEN® (Boston, MA). Liberase Blendzyme 3 (0.038 WU/ml) and Complete Protease Inhibitor Cocktail were from Roche (Basel, Switzerland). Culture plates and flasks were from Corning (Corning, NY). Glass-bottom six-well plates were from MatTek (Ashland, MA). Ninety six-well Scintiplate®, UniFilter® micro plate, Isoplate® scintillation plate, and OptiPhase Supermix were obtained from PerkinElmer (Shelton, CT). Ultracentrifugation tubes were from Beckman Coulter Inc. (#344062; Brea, CA). TLC plates (Silica gel 60) were from Merck Millipore (Billerica, MA). Atglistatin was from Xcess Biosciences (San Diego, CA). CAY10499 was from Cayman Chemical (Ann Arbor, MI). TG PAP 150-kit (#61236) was obtained from BioMerieux (Marcy l'Etoile, France). SYBR Master Mix was from Kapa Biosystems (Wilmington, MA). Criterion or Mini-Protean® TGX™ gels (4–20%), Clarity™ Western ECL Substrate, and the goat anti-rabbit HRP-conjugated (HRP) secondary antibody #1706515 were purchased from Bio-Rad (Copenhagen, Denmark). Pierce™ BCA protein assay kit was from Thermo Fisher Scientific (Rockford, IL).

Antibodies against total thymoma viral proto-oncogene/AKT serine/threonine kinase (Akt) (#9272, rabbit polyclonal antibody), phosphorylated Akt (pSer473, #9271, rabbit polyclonal antibody), Slc2a1/Glut1 (#12938, rabbit monoclonal antibody), Pkm (#3106, rabbit monoclonal antibody), Pdha1 (#3205, rabbit monoclonal antibody), and β-actin (#4970, rabbit monoclonal antibody) were from Cell Signaling Technology (Beverley, MA). Antibody against Pdha1-p300 (#ABS194, rabbit polyclonal antibody) was from Millipore. Antibodies against muscle-associated glycogen phosphorylase (Pygm) (#ab81901, rabbit polyclonal antibody) and Pdk4 (#214938, rabbit monoclonal antibody) were from Abcam (Cambridge, UK). Antibody against Gapdh (#sc-25778, rabbit polyclonal antibody) was obtained from Santa Cruz Biotechnology (Dallas, TX). The goat anti-rabbit HRP-conjugated secondary antibody #111-035-144 was from Jackson ImmunoResearch (Suffolk, UK). All chemicals used were of standard commercial high-purity quality.

Generation of the Plin2 null mice

A BAC clone containing the *Plin2* genetic locus (AB2.2 ES cells, strain 129S7/SvEvBrd-Hprtb-m2, clone #bMQ-28H12) was modified with recombineering to generate a floxed *Plin2* targeting vector. Because the Plin2 protein is rapidly degraded in the absence of LD targeting (31), *LoxP* sites were inserted in intron 3 and intron 6 of the *Plin2* gene to flank exon sequences that are essential for targeting of the Plin2 protein to LD surfaces. With this design, any potential truncated Plin2 protein sequence translated from the genetically modified gene would be expected to untarget from LDs and be rapidly degraded. The specific details for generation of the targeting vector will be published elsewhere (Y.K.L., K.T.D., and A.R.K., unpublished observations). Standard homologous recombination in 129/SvJEv embryonic stem (ES) cells was used to target the *Plin2* gene. Resulting chimeric mice were bred with C57BL/6J mice (Jackson Laboratory, Bar Harbor, ME) for germline transmission. The resulting *Plin2* floxed line on a mixed B6.129/Sv background was subsequently crossed with mice expressing MMTV-Cre recombinase (Jackson Laboratory) to generate *Plin2* null mice ($Plin2^{-/-}$). The floxed *Plin2* mice were generated in compliance with the guidelines given by the Animal Care and Use Committee of the National Institutes of Health under a Division of Intramural Research, National Institute of Diabetes and Digestive and Kidney Diseases, under approved animal study protocol K039-LCDB.

Animal experiments

$Plin2^{+/+}$ and $Plin2^{-/-}$ mice were housed in a temperature-controlled (22°C) facility with a strict 12-h light/dark cycle. Male mice backcrossed for 10 generations into C57BL/6N (Janvier Labs, Le Genest-Saint-Isle, France) were given standard chow (#RM3-801190, SDS diets, consisting of 12% calories from fat, 27% from protein, and 61% from carbohydrate) until 12 weeks of age. Mice were euthanized by cervical dislocation at 8:00 to 10:00 AM, and tissues were snap-frozen in liquid nitrogen and stored at −80°C until further analysis. All animal use was approved and registered by the Norwegian Animal Research Authority (NARA, under animal study protocols FOTS IDs: #6305 and #6922) and conformed to the guidelines from Directive 2010/63/EU of the European Parliament on the protection of animals used for scientific purposes.

Isolation of satellite cells

Female siblings (14 weeks) backcrossed into C57BL/6N for six generations were used for primary satellite cell isolation from the hind leg containing musulus gastrocnemius and musculus soleus. Primary muscle satellite cells (myoblasts) were isolated and purified, as has been previously described (32). Briefly, the muscle tissue was incubated with 2% collagenase II at 37°C for 90 min to enzymatically dissociate the cells. Satellite cells were liberated by further digestion with Blendzyme at 37°C for 30 min. To enrich myoblasts, we split the cell population in DPBS with no trypsin or EDTA. Further enrichment of myoblasts was obtained by preplating for 15 min on collagen-coated flasks. This tends to leave behind cells that stick quickly, which are predominantly fibroblasts. Fibroblasts tend to be very flat when grown on collagen, whereas myoblasts are more compact and smaller in diameter. In addition, the F-10-based primary myoblast growth medium gives myoblasts a growth advantage over fibroblasts. $Plin2^{+/+}$ and $Plin2^{-/-}$ myotube cultures were considered established when fibroblasts were no longer visible in the cultures.

Cell culture and stimulation of myotubes

Purified myoblasts were proliferated on standard plasticware coated with collagen (0.01%). To enhance myotube formation, Matrigel (diluted 1:50 in DMEM) was used as coating when myoblasts were seeded to differentiate into myotubes. Mouse myoblasts were grown to subconfluence in DMEM/Ham's F-10 (1:1, 5.5 mM glucose) supplemented with 20% FBS, 5 ng/ml basic fibroblast growth factor, 25 IU penicillin, 25 μg/ml streptomycin, and 1.25 μg/ml amphotericin B at 37°C in 5% CO_2. At ∼80% confluence, growth medium was replaced by DMEM supplemented with 2% horse serum and antibiotics to induce fusion of myoblasts into multinucleated myotubes. Unless otherwise stated, cells differentiated for 4 days were used in experiments.

OA was bound to FA-free BSA with an OA:BSA ratio of 2.5:1 in all experiments (further referred to as OA). Control myotubes and OA-stimulated myotubes received the same concentration of BSA. The lipase inhibitors (Atglistatin and CAY10499) were solved in DMSO and diluted in medium to a final concentration of 0.1% DMSO. Control myotubes and lipase inhibitor-stimulated myotubes received the same concentration of DMSO.

To measure insulin response, we incubated myotubes differentiated for 3 days in medium containing OA (100 μM) for 24 h. Myotubes were subsequently incubated with glucose-free DMEM medium for 2 h in the presence of OA (100 μM), followed by 15-min incubation in DMEM (5.5 mM glucose) in the presence or absence of insulin (100 nM). Myotubes from two wells (six-well plate) were pooled in RIPA buffer, supplemented with Complete Protease Inhibitor cocktail, and stored at −80°C until further analysis. Protein content in cell extracts was measured by Pierce™ BCA protein assay kit.

Immunoblotting

Cell extracts were sonicated briefly, as has been described previously (33). Proteins (15 μg) were mixed with Laemmli buffer and separated on a 4%–20% Criterion or Mini-Protean® TGX™ gels, followed by blotting to nitrocellulose or PVDF membranes. Membranes were immunoblotted with the following antibodies: rabbit anti-mouse Plin2 [(31); #N510; 3 μg/ml], rabbit anti-mouse Plin3 [(34); 10 μg/ml], rabbit anti-mouse Plin4 and rabbit anti-mouse Plin5 [(33); 10 μg/ml], rabbit anti-human glucose transporter 1 (Slc2a1/Glut1, 1:1,000), rabbit anti-human pyruvate kinase (Pkm, 1:1,000), rabbit anti-human Pygm (1:1,000), rabbit anti-mouse pyruvate dehydrogenase kinase 4 (Pdk4, 1:1,000), rabbit anti-human muscle pyruvate dehydrogenase α 1 (Pdha1, 1:1,000), rabbit anti-human phosphorylated muscle pyruvate dehydrogenase α 1 (Pdha1-p300, 1:1,000), total Akt kinase (detects isoforms Akt1-3, 1:1,000), Ser473-phosphorylated Akt (1:1,000), GAPDH (Gapdh, 1:500), and β-actin (1:1,000), followed by HRP-labeled secondary antibodies (∼1:10,000). Immunoreactive bands were detected with Clarity™ Western ECL Substrate, visualized with ECL using Chemidoc XRS (Bio-Rad), and quantified with

Image Lab software (version 4.0). The β-actin signal was used to normalize for protein loading.

Preparation and analysis of RNA

Cells were lysed in Nucleic Acid Purification Lysis Solution:PBS (1:1) and frozen at −80°C before isolation. Total RNA from cell extracts was isolated on a ABI 6100 Nucleic Acid Prep-Station with the preprogrammed "RNA-Cell method." RNA quality and quantity were determined with NanoDrop ND-1000 Spectrophotometer (Thermo Fisher Scientific, Waltham, MA). Reverse transcription quantitative real-time PCR (RT-qPCR) was performed in two steps. First, total RNA (20 ng/μl) was reverse-transcribed into single-stranded complementary DNA with random hexamers and Superscript III RT (50°C for 60 min and 72°C for 15 min). Next, gene-specific regions (70–120 bp) were amplified from complementary DNA (10 ng) with assay primers (100 nM each) and KAPA SYBR Fast Master Mix (10-μl reaction, 95°C for 3 min, followed by 40 cycles; 95°C for 10 s and 60°C for 20 s) on the ABI 7900HT instrument (Applied Biosystems, Thermo Fisher Scientific, Waltham, MA). Assay primers (Tm = 60) were designed with Primer-BLAST software (35). All assay primer pairs were designed to bind to adjacent exons spanned by a large intron with amplicon sizes ranging from 70 to 110 nt. Primers used are listed in **Table 1**. Data were analyzed with relative quantification (ΔΔCq method). Results are presented as gene expression in relation to endogenous control ($2^{-\Delta\Delta Cq}$). TATA-box binding protein (*Tbp*) mRNA was verified to not differ in expression among groups or treatments and was used as endogenous control in all experiments.

Microscopy

Myoblasts seeded on Matrigel-coated six-well glass-bottom dishes were differentiated into myotubes for 3 days before switching to media supplemented with OA (100 μM) for 24 h. For live imaging, LDs were stained by incubating myotubes with Bodipy 493/503 (2 μg/ml) for 10 min, followed by nuclei staining with Hoechst 33258 (2.5 μg/ml) for 15 min. Live images were randomly taken in 25 positions per well with a ×20 objective on an Olympus IX81 inverted fluorescence Scan^R platform (Olympus Corporation, Tokyo, Japan), as has been previously described (36). After gating out aggregates and dead cells, each parameter was determined from an average 150 images per donor group (average of 96 ± 25 nuclei per image). For confocal pictures, myotubes were fixated for 1 h with 4% PFA in 100 mM of phosphate buffer (pH 7.4), washed and stained with Bodipy 493/503 (1 μM) and Hoechst 33342 (5 μM) for 20 min. Pictures were taken with a ×40 objective on a LSM 710 confocal microscope (Zeiss, Oberkochen, Germany).

FA accumulation and lipolysis assay

Accumulation (real-time uptake) and lipolysis (efflux) of FA were measured with scintillation proximity assay, as has been previously described (37). In this method, the radiolabeled substrates taken up will accumulate in the adherent cells and become concentrated close to the scintillator embedded in the plastic bottom of each well and provide a stronger radioactive signal than would the radiolabel dissolved in the medium alone. Cells were seeded and differentiated for 3 days in 96-well Scintiplate® coated with Matrigel. To determine OA uptake and accumulation, we gave myotubes fresh medium comprising DMEM without phenol red, supplemented with [1-^{14}C]OA (0.5 μCi/ml) and unlabeled OA (final OA concentration 100 or 400 μM) in the presence of DMSO (0.1%) or the ATGL inhibitor Atglistatin [10 μM (38)]. Lipid accumulation was monitored regularly for the next 24 h on a 2450 MicroBeta^2 scintillation counter (PerkinElmer, Shelton, CT). Thereafter, to measure FA efflux (lipolysis), the labeled myotubes were washed twice with PBS containing 0.5% BSA before the myotubes were incubated in DPBS supplemented with 10 mM HEPES, 0.5% BSA, and 100 μM glucose. The decline in accumulated [1-^{14}C]OA was measured at 0, 2, 4, and 6 h.

Glucose and FA substrate oxidation assays

Cells were seeded and differentiated in 96-well plates coated with Matrigel solution and subjected to substrate oxidation assay, as has been described previously (37). To measure FA oxidation

TABLE 1. Primers used for RT-qPCR in this study

Gene	Forward Primer	Reverse Primer	Amplicon Size
Acadl	CGGAAGCTGCATAAGATGGGA	AGCTGGCAATCGGACATCTT	75
Acadm	TGGATTCATTGTGGAAGCCGA	CCTCTGGTGTCAGAGCATCG	87
Acadvl	GCATTTGGCCTGCAAGTACC	AATCTCTGCCAAGCGAGCAT	78
Acox1	AATCTGGAGATCACGGGCACTT	GTCTTGGGGTCATATGTGGCAG	95
Cd36	AGGCATTCTCATGCCAGTCG	TGTACACAGTGGTGCCTGTT	119
Cpt2	TATGATGGCTGAGTGCTCCAA	CCGTAGAGCAAACAAGTGTCG	91
Fabp3	GGACAGCAAGAATTTTGATGACTAC	TTGGTCATGCTAGCCACCTG	78
Gys1	TTGGGGTCTTCCCCTCCTAC	GTGGAGATGCTGGGGATGC	82
Hk1	GGACCACAGTTGGCGTAGA	CTCAGGGTCTTGTGGAACCG	76
Hk2	CTTCCCTTGCCAGCAGAACA	TGACCACATCTTCACCCTCG	95
Pdha1	CGTGGTTTCTGTCACTTGTGTG	CGTAGGGTTTATGCCAGCCT	72
Pdk4	AAGATGCTCTGCGACCAGTA	CAATGTGGATTGGTTGGCCTG	91
Pkm	GAAACAGCCAAGGGGGACTAC	CACAAGCTCTTCAAACAGCAGAC	108
Plin2 (exon4-5)	GGGCTAGACAGGATGGAGGA	CACATCCTTCGCCCCAGTTA	99
Plin2 (exon7-8)	GTGGAAGAGAAGCATCGGCT	GGCGATAGCCAGAGTACGTG	82
Plin3	CGAAGCTCAAGCTGCTATGG	TCACCATCCCATACGTGGAAC	98
Plin4	ACCAACTCACAGATGGCAGG	AGGCATCTTCACTGCTGGTC	109
Plin5	GGTGAAGACACCACCCTAGC	CCACCACTCGATTCACCACA	115
Ppara	ACTACGGAGTTCACGCATGT	GTCGTACACCAGCTTCAGCC	74
Pparg	TTGCTGTGGGGGATGTCTCAC	AACAGCTTCTCCTTCTCGGC	70
Ppard	ACATGGAATGTCGGGTGTGC	CGAGCTTCATGCGGGATTGTC	108
Ppargc1a	AGTCCCATACACAACCGCAG	CCCTTGGGGGTCATTTGGTGA	94
Pygm	GAGTGGAGGACGTGGAAAGG	CCGAAGCTCAGGAATTCGGT	77
Slc2a1	CTCGGATCACTGCAGTTCGG	CGTAGCGGTGGTTCCATGTT	97
Slc2a4	CGACGGACACTCCATCTGTT	ACATAGCTCATGGCTGGAACC	104
Tbp	AGCCTTCCACCTTATGCTCAG	GCCGTAAGGCATCATTGGACT	90
Ucp2	TTGGCCTCTACGACTCTGTCA	CAGGGCACCTGTGGTGCTA	98
Ucp3	CTACAGAACCATCGCCAGGGA	GTCGTAGGTCACCATCTCAGCA	109

from prelabeled intracellular lipid pools, we incubated myotubes with [1-^{14}C]OA (0.5 μCi/ml) and unlabeled OA (final OA concentration, 100 or 400 μM) for 24 h, combined with various treatments (0.1% DMSO, 10 μM CAY10499 or 10 μM Atglistatin). Myotubes were then washed twice with PBS containing 0.5% BSA and given DPBS media supplemented with 10 mM HEPES, 10 μM BSA, and 1 mM L-carnitine to capture CO_2. To measure glucose oxidation, we gave myotubes D-[^{14}C(U)]glucose (0.58 μCi/ml) and unlabeled glucose (final glucose concentration 200 μM) directly in the CO_2-capturing media (DPBS supplemented with 10 mM HEPES, 10 μM BSA, and 1 mM L-carnitine). A 96-well UniFilter® microplate, activated for capture of CO_2 by the addition of 1 M NaOH, was subsequently mounted on top of the 96-well plate, and the sandwich was incubated at 37°C for 4 h. [^{14}C]CO_2 captured in the filter was counted by liquid scintillation on a 2450 MicroBeta^2 scintillation counter (PerkinElmer, Shelton, CT) as a measure of produced CO_2. After CO_2 capturing, myotubes were washed with PBS and lysed with 0.1 M NaOH before cell-associated radioactivity (accumulated substrate) was determined by liquid scintillation. Acid-soluble metabolites (ASMs) in the media were measured, as has been previously described (36). ASMs consist of β-oxidation and tricarboxylic acid cycle metabolites and reflect incomplete FA or glucose oxidation in the mitochondria.

Lipid droplet isolation

Cells from six 10-cm petri dishes were stimulated with 200 μM of OA for 24 h, washed twice with cold PBS, harvested in suspension buffer (25 mM tricine pH 7.8, 8.6% sucrose, and Complete Protease Inhibitor cocktail), mixed gently, and frozen at −80°C. To disrupt cells, samples were thawed slowly in ice-water slurry for ∼30 min and transferred to a precooled N_2 cell-disruption vessel (#4639, Parr Instrument Co., Moline, IL). Samples were exposed to 600 psi N_2 for 20 min, then released slowly (dropwise) into a 15-ml tube. The disrupted cell lysate was subsequently centrifuged for 10 min at 3,000 *g* at 4°C to remove nuclei and undisrupted cell debris. The suspension containing LDs was adjusted to 2 ml and transferred to the bottom of an ultracentrifugation tube, followed by a second layer consisting of 1.8 ml of wash buffer (20 mM HEPES pH 7.4, 100 mM KCl, 2 mM $MgCl_2$, and 4% sucrose [w/v]), and a top layer of 0.4 ml of collection buffer (20 mM HEPES pH 7.4, 100 mM KCl, and 2 mM $MgCl_2$). Tubes were balanced and centrifuged for 60 min in a SW60Ti rotor at 200,000 *g* at 4°C in a XL-90 Ultracentrifuge (Beckman Coulter Inc.). The top layer (∼0.4 ml) was isolated with a tube slicer prior to the collection of floating LDs.

Lipid composition of isolated LDs

Isolated LDs were mixed with ×2 volume of chloroform:heptane:methanol (4:3:2, v/v/v) and lipids extracted by thoroughly mixing for 1–2 min prior to centrifugation for 5 min at 2,000 *g*. The lower organic phase was carefully transferred into a glass tube and evaporated under N_2 before lipids were dissolved in chloroform:methanol (2:1, v/v). TAG content in samples was determined with TG PAP 150 kit, adjusted to 250 ng TAG/μl, and stored at −20°C under argon. The TLC plate was fully developed in methanol:ethyl acetate (6:4, v/v) to remove impurities, then dried for 6–8 min at 40°C. Lipid samples (1 μg TAG) and lipid standard mix (equal weights of TAG, DAG, MAG, PL, FFA, CE, and free cholesterol) were spotted on the plate and air-dried briefly, and the plate was developed in heptane:diethyl ether:acetic acid (55:45:1, v/v/v). The plate was subsequently dried for 10 min at 40°C and developed with copper sulfate staining (39) by exposing the plate to a developing reagent consisting of 10% $CuSO_4 \times 5H_2O$ (w/v) and 8% H_3PO_4 in H_2O (v/v) for ∼40 s. Excess solution was removed by decanting, and the back of the plate was cleaned with tissue paper.

The plate was subsequently air-dried briefly, placed on a heating plate for 10 min at 60°C, and then for 10 min at 150°C. After being cooled down, the plate was scanned with an Epson Perfection V700 image scanner (Seiko Epson Corporation, Nagano, Japan).

Lipid distribution in cells

Myotubes were incubated with [1-^{14}C]OA (0.5 μCi/ml) and unlabeled OA (final OA concentration 100 or 400 μM) for 24 h. The myotubes were washed twice with PBS and harvested with two additions of 125 μl dH_2O. Cellular lipid distribution was analyzed as has been previously described (40). Briefly, homogenized cell fractions were extracted, lipids were separated by TLC with hexane:diethyl ether:acetic acid (65:35:1, v/v/v) as developing solvent, and radioactivity in excised bands was quantified by liquid scintillation (Packard TriCarb 1600, PerkinElmer, Shelton, CT).

Triacylglycerol measurements

Myotubes were incubated with OA alone (100 μM) or in the presence of Atglistatin (10 μM) for 24 h. Thereafter, the myotubes were washed with PBS and harvested in PBS or RIPA buffer (50 mM Tris-HCl pH 7.4, 150 mM NaCl, 1% NP-40, 0.5% sodium deoxycholate, 0.1% SDS, and 2 mM EDTA). Measurement of cellular TAG was performed with the TG PAP 150 kit according to the supplier's protocol.

Glycogen synthesis

Myotubes were incubated in DMEM without glucose, supplemented with D-[^{14}C(U)]glucose (0.5 μCi/ml), unlabeled glucose (final glucose concentration 1 mM), pyruvate (1 mM), and BSA (10 μM) in the presence or absence of insulin (100 nM) for 3 h to measure glycogen synthesis. The myotubes were washed twice with PBS and harvested in KOH (1 M). After protein measurements, glycogen (final concentration 20 mg/ml) and more KOH (final concentration 4 M) were added to the samples. Thereafter, D-[^{14}C(U)]glucose incorporated into glycogen was measured as has been previously described (36).

Statistical methods

Values are presented as means ± SEM unless stated otherwise. The value *n* represents the number of experiments performed with at least duplicate samples. Two-tailed unpaired *t* tests were performed to determine the difference between groups (*Plin2*$^{+/+}$ and *Plin2*$^{-/-}$) with GraphPad Prism 5.0 Software (GraphPad Software Inc., San Diego, CA), whereas two-tailed paired *t* tests were performed to determine effects of treatments. Linear mixed-model analysis (SPSS 20.0.0.1, IBM SPSS Inc., Chicago, IL) was used to compare *Plin2*$^{+/+}$ and *Plin2*$^{-/-}$ myotubes in the time-course FA accumulation and lipolysis experiments (scintillation proximity assay). *P* < 0.05 was considered statistically significant.

RESULTS

Establishment of myotube cultures lacking Plin2

To investigate the functional role of Plin2 in myotubes, we first generated mice with homozygous disruption of the *Plin2* gene by deleting exons 4, 5, and 6 that are essential for functional targeting of Plin2 to LD surfaces. A thorough phenotypic characterization of *Plin2*$^{-/-}$ mice will be published elsewhere (Y.K.L., K.T.D., and A.R.K, unpublished observations). Hind legs from female *Plin2*$^{+/+}$ and *Plin2*$^{-/-}$ littermates, backcrossed into C57BL/6N for six generations, were used to isolate primary muscle satellite cells and establish *Plin2*$^{+/+}$ and *Plin2*$^{-/-}$ myoblast cultures. The *Plin2*$^{+/+}$

and $Plin2^{-/-}$ myoblast populations differentiated equally well into myotubes on the basis of the presence of multi-nuclear fiber-like cells, observed by microscopic inspection (**Fig. 1A**) and by the comparable reduction in mRNA expression of the nonmyotube satellite cell marker paired box 7 (*Pax7*) (Fig. 1B). The structural *Plin2* gene differences in the $Plin2^{+/+}$ and $Plin2^{-/-}$ myotubes were validated by RT-qPCR. Primers that recognize sequences within deleted exons 4 to 5 failed to amplify mRNA target sequences from $Plin2^{-/-}$ myotubes (Fig. 1C), confirming that these myotubes lack functional full-length *Plin2* mRNA. Primers amplifying across the retained exon 7 to 8 junction showed lower expression of the truncated $Plin2^{-/-}$ mRNA ($\sim15\%$) compared with wild-type *Plin2* mRNA (Fig. 1C). We next determined whether ablation of *Plin2* was compensated for by increased expression of other *Plin* genes in myotubes. *Plin3* mRNA expression was slightly ($\sim40\%$) reduced, *Plin4*

mRNA was unchanged, whereas *Plin5* mRNA expression was increased (~5-fold) in $Plin2^{-/-}$ compared with $Plin2^{+/+}$ myotubes (Fig. 1D). Judged by mRNA levels in relation to *Tbp*, *Plin4* and *Plin5* mRNAs in the cultured myotubes were considerably lower ($<1\%$) than *Plin2* and *Plin3* mRNAs in cultured wild-type myotubes.

Next, we analyzed Plin protein content. Plin2 immuno-signals with an expected molecular mass of ~50 kDa were observed in $Plin2^{+/+}$ myoblasts and myotubes (Fig. 1E), whereas the signal was absent in $Plin2^{-/-}$ myotubes, which confirms correct genetic ablation of the *Plin2* gene. We observed a significant decline in Plin2 protein levels when $Plin2^{+/+}$ myoblasts were differentiated into myotubes, whereas Plin3 protein content was essentially unchanged by differentiation, regardless of genotype (Fig. 1E). Less distinct protein bands were observed for the very weakly transcribed Plin4 and Plin5 (results not shown). Hence,
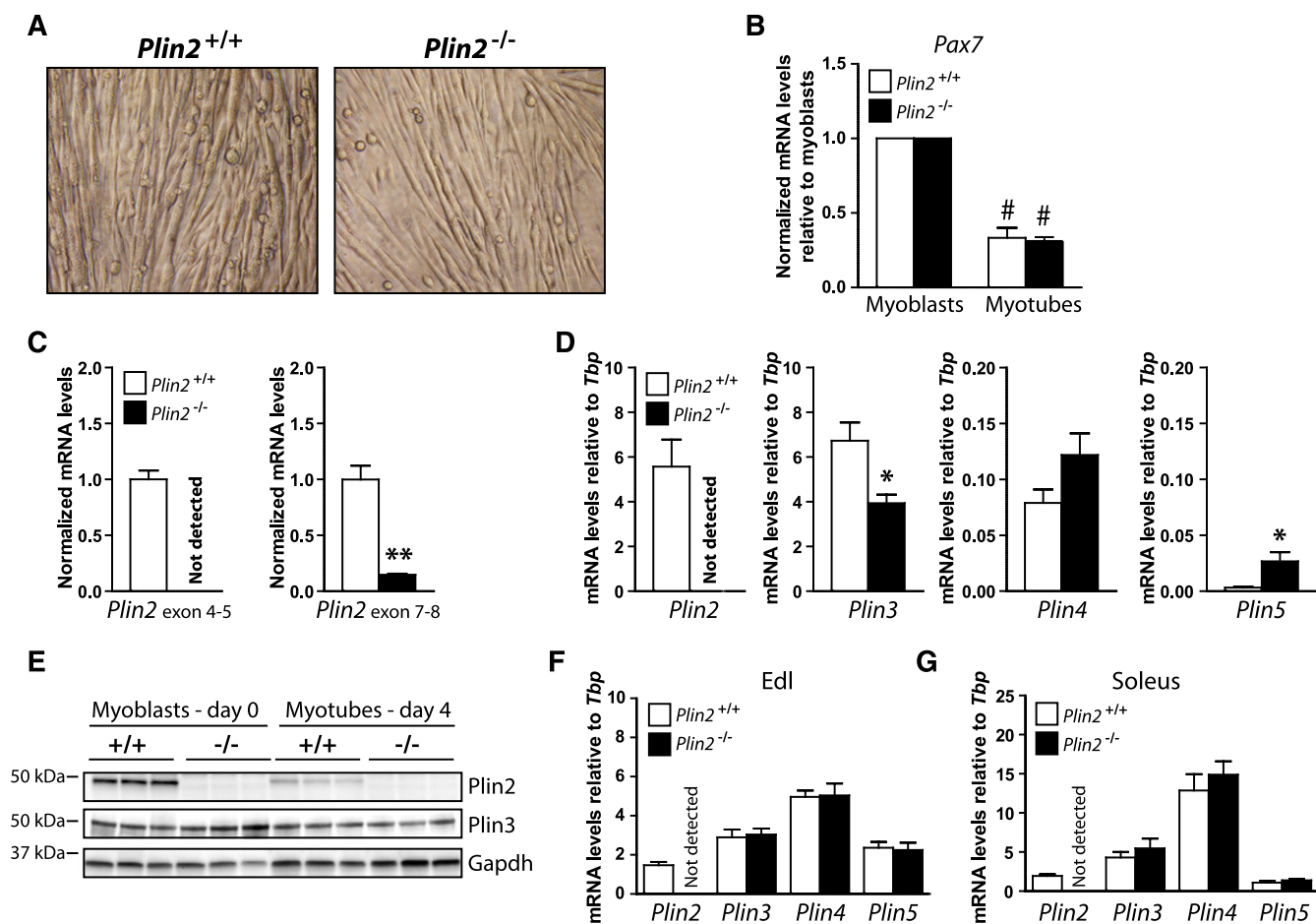

Fig. 1. Expression of Plins in muscle and established $Plin2^{+/+}$ and $Plin2^{-/-}$ myotubes and myoblasts. Primary muscle satellite cells (myoblasts) were isolated from the hind leg of $Plin2^{+/+}$ and $Plin2^{-/-}$ mice. A: Established $Plin2^{+/+}$ and $Plin2^{-/-}$ myoblast cultures differentiated equally well into multinucleated myotubes. B: Expression of *Pax7* mRNA in relation to the expression of TATA-box binding protein (*Tbp*) determined by RT-qPCR. The results are presented normalized to the expression levels in undifferentiated myoblasts. C: RT-qPCR with primers amplifying across the *Plin2* exon 4–5 junction and the *Plin2* exon 7–8 junction in relation to the expression of *Tbp* and normalized to the expression levels in $Plin2^{+/+}$ myotubes, confirmed the absence of exon 4-6 *Plin2* mRNA sequences in $Plin2^{-/-}$ myotubes. D: Expression of *Plin2*, *Plin3*, *Plin4*, and *Plin5* mRNAs determined by RT-qPCR in relation to the expression of *Tbp*. Results in B–D are presented as means ± SEM (n = 3–6, *$P < 0.05$ and **$P < 0.01$ vs. $Plin2^{+/+}$ myotubes, #$P < 0.05$ vs. myoblasts). E: Expression of Plin2 and Plin3 proteins in myoblasts (day 0) and differentiated myotubes (day 4). The membrane contains samples from three independent experiments (n = 3). F: Relative mRNA expression of *Plin2*, *Plin3*, *Plin4*, and *Plin5* in extensor digitorum longus of chow-fed 12-week-old $Plin2^{+/+}$ and $Plin2^{-/-}$ male mice. G: Relative mRNA expression of *Plin2*, *Plin3*, *Plin4*, and *Plin5* in soleus. Gene expression levels in F and G were determined by RT-qPCR and are presented in relation to the expression of *Tbp* as means ± SEM (n = 9 in each group). Edl, extensor digitorum longus; Pax7, paired box 7.

the lack of Plin2 in cultured $Plin2^{-/-}$ myotubes was not compensated for by elevated mRNA expression or accumulation of other Plin proteins.

We also examined mRNA levels of *Plins* in extensor digitorum longus and soleus muscle fibers dissected from chow-fed $Plin2^{+/+}$ and $Plin2^{-/-}$ mice. Disruption of *Plin2* did not alter expression of other *Plin* mRNAs (Fig. 1F, G). Furthermore, *Plin2* and *Plin3* mRNA levels were similar in myotubes and the two muscle fibers, whereas the expression of *Plin4* and *Plin5* mRNAs was more elevated in the muscle fibers than in the cultured myotubes. Thus, the $Plin2^{+/+}$ and $Plin2^{-/-}$ myotube cultures represent an important parallel model to analyze Plin2 function for muscle metabolism, allowing for defined biochemical benchmarkings that are not readily accessible in situ.

Reduced accumulation of lipids in the absence of Plin2

OA is easily taken up by cells and esterified into TAG that is incorporated into LDs, and thus, incubation with OA is an efficient strategy to promote LD formation and monitor relative intracellular lipid storage. $Plin2^{+/+}$ myotubes cultured with 100 µM OA for 24 h increased Plin2 mRNA and protein content considerably compared with cells cultured with BSA (**Fig. 2A**, B) but had no effect on mRNA (results not shown) and protein expression of Plin3 (Fig. 2B). To determine whether removal of a functional Plin2 in myotubes affected the ability to store lipids, we incubated

$Plin2^{+/+}$ and $Plin2^{-/-}$ myotubes with 100 µM OA for 24 h before LDs were stained with Bodipy 493/503 (green) and nuclei stained with Hoechst 33258 (blue). A marked reduction in accumulated LDs was observed in $Plin2^{-/-}$ compared with $Plin2^{+/+}$ myotubes (Fig. 2C). There were fewer quantified LDs per nucleus, observed under a ×20 objective, in $Plin2^{-/-}$ than in $Plin2^{+/+}$ myotubes (Fig. 2D). Because smaller LDs are not necessarily labeled and recognized with automatic quantification, we also determined lipid distribution after incubation with $[1\text{-}^{14}C]OA$ for 24 h. $Plin2^{-/-}$ myotubes incorporated less OA into TAG (Fig. 2E) and DAG (Fig. 2F) and contained lower levels of FFAs (Fig. 2G) than did $Plin2^{+/+}$ myotubes. Incorporation into phospholipids (Fig. 2H) and cholesteryl esters (results not shown) was unaffected by removal of *Plin2*. These observations demonstrate that $Plin2^{-/-}$ myotubes exposed to FAs store reduced levels of LDs compared with $Plin2^{+/+}$ myotubes.

Absence of Plin2 reduced accumulation of lipids by increasing lipolysis

To mechanistically determine why myotubes lacking Plin2 accumulated less TAG-containing LDs, we followed OA accumulation in the myotubes for 24 h. During the first ∼4 h, $Plin2^{+/+}$ and $Plin2^{-/-}$ myotubes accumulated similar levels of $[1\text{-}^{14}C]OA$, but total accumulation after 24 h was lower in $Plin2^{-/-}$ myotubes incubated with 100 µM OA (**Fig. 3A**, $P < 0.05$) or 400 µM OA (Fig. 3B, $P = 0.06$) than in $Plin2^{+/+}$
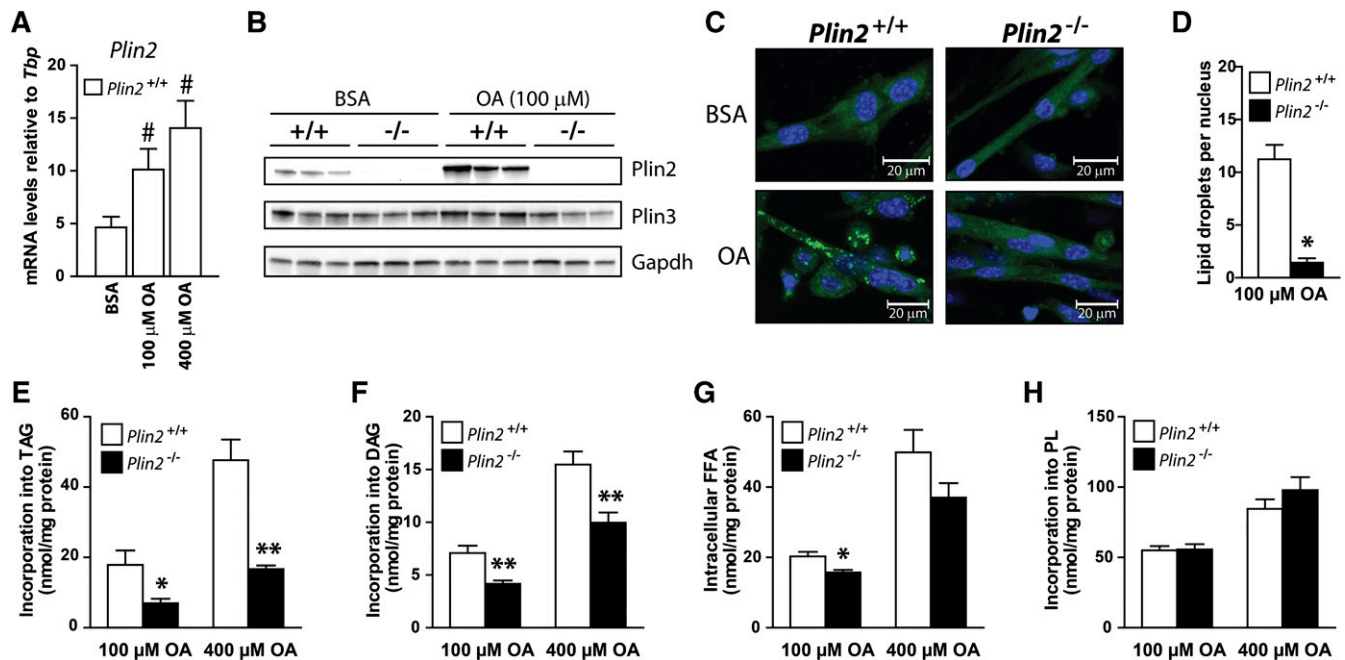

Fig. 2. Lipid storage and distribution in $Plin2^{+/+}$ and $Plin2^{-/-}$ myotubes. A–D: Myotubes were incubated for 24 h with BSA (40 µM) or OA (100 or 400 µM OA). A: Relative expression of *Plin2* mRNA determined by RT-qPCR normalized to the expression of TATA-box binding protein (*Tbp*). Results are presented as means ± SEM (n = 3, $^{\#}P < 0.05$ vs. BSA). B: Expression of Plin2 and Plin3 proteins in myotubes. C: Lipid droplets (LDs) in $Plin2^{+/+}$ and $Plin2^{-/-}$ myotubes were labeled with fluorescent dyes sequestering in neutral LDs (Bodipy 493/503, green) or nuclei (Hoechst 33342, blue). Representative confocal images are presented (×40 objective; inserted bars are 20 µm). D: Another set of images were acquired with a ×20 objective with an Olympus IX81 fluorescence microscope. Images were analyzed by Scan^R analytical software by comparing the number of stained LDs in relation to the number of nuclei per image, with an average total of 150 images per parameter. Results are presented as means ± SEM (n = 3, $*P < 0.05$ vs. Plin2 $^{+/+}$). E–H: Myotubes were preincubated for 24 h with $[1\text{-}^{14}C]OA$ to label accumulated lipids. The content of radiolabeled TAG (E), DAG (F), FFA (G), and PL (H) in myotubes was determined by TLC and related to cellular protein content. The results are presented as means ± SEM (n = 6, $*P < 0.05$, $**P < 0.01$ vs. $Plin2^{+/+}$).

myotubes. In contrast, coincubation with Atglistatin (38), a reversible inhibitor of ATGL that catalyzes the first and rate-limiting step in lipolysis of TAG, increased accumulation of OA in $Plin2^{-/-}$ myotubes, in a manner similar to that of $Plin2^{+/+}$ myotubes (Fig. 3C, D). Coincubation with Atglistatin increased cell-associated [1-^{14}C]OA in $Plin2^{-/-}$ myotubes compared with DMSO with a more pronounced effect, with higher OA concentration (Fig. 3E). Myotubes cultured in 100 µM OA coincubated with the ATGL and HSL inhibitor CAY10499 (41, 42) alone or in combination with Atglistatin increased cell-associated [1-^{14}C]OA only in $Plin2^{-/-}$ myotubes (Fig. 3F). These results suggest that there were constantly higher ATGL and HSL lipolytic activities in $Plin2^{-/-}$ myotubes than in $Plin2^{+/+}$ myotubes.

Lipolytic rates are difficult to normalize between two cell populations with differences in LD content. To overcome this, we utilized our established culture conditions using Atglistatin to minimize TAG differences between the $Plin2^{+/+}$ and $Plin2^{-/-}$ myotubes. Whereas $Plin2^{-/-}$ myotubes cultured with 100 µM OA alone accumulated less TAG than did $Plin2^{+/+}$ myotubes (**Fig. 4A**), a combination of OA and Atglistatin resulted in TAG levels (Fig. 4A) and LD content (Fig. 4B) in $Plin2^{-/-}$ myotubes that were similar to those in $Plin2^{+/+}$ myotubes. These latter $Plin2^{+/+}$ and $Plin2^{-/-}$ myotubes were

then washed to remove the exogenous OA and Atglistatin before measurement of lipolysis. Lipolysis, measured as a loss of [1-^{14}C]OA accumulated in the myotubes, was consistently overall higher in $Plin2^{-/-}$ myotubes than in $Plin2^{+/+}$ myotubes (Fig. 4C, D). To compare the lipid composition of the stored LDs, we stimulated $Plin2^{+/+}$ and $Plin2^{-/-}$ myotubes with 200 µM OA alone or coincubated with Atglistatin for 24 h prior to LD isolation. LD preparations containing the same amount of TAG (1 µg) were subsequently separated with TLC, and various lipid species were identified with copper sulfate staining. LDs isolated from OA-stimulated $Plin2^{-/-}$ myotubes stained stronger for lipolytic degradation products such as DAG, MAG, and FFA than did those from $Plin2^{+/+}$ myotubes (Fig. 4E, F), whereas inhibition of lipolysis by coincubation with Atglistatin lowered the relative staining (Fig. 4F). These differences further supported the notion that disruption of $Plin2$ in cultured myotubes resulted in LDs prone to lipolytic attack.

Absence of Plin2 increased FA oxidation

An important biological role for cytosolic LDs is to store energy-rich FAs that may be mobilized for energy production when needed. We were interested to determine whether the reduced LD stores in myotubes affected FA oxidation
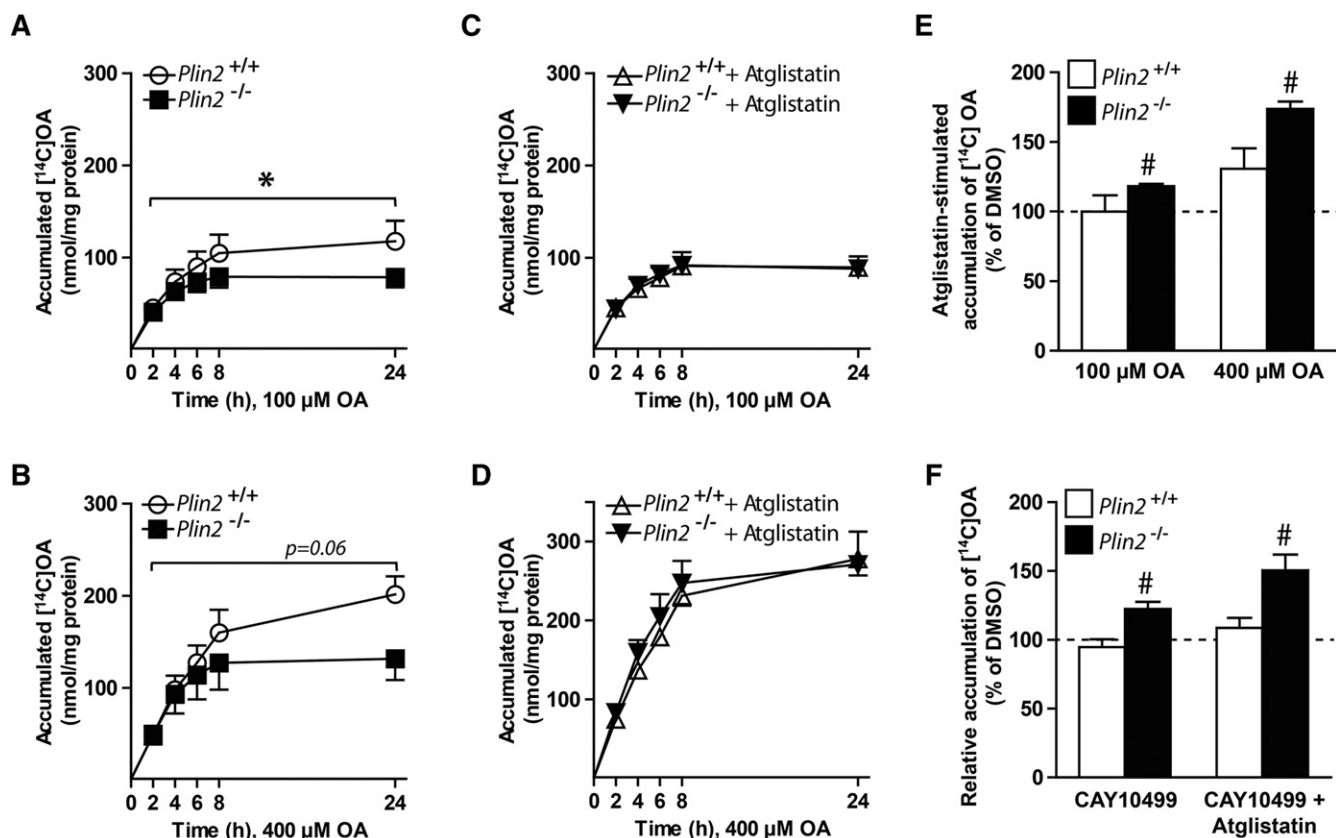
Fig. 3. Accumulation of oleic acid in $Plin2^{+/+}$ and $Plin2^{-/-}$ myotubes. Myotubes were incubated with [1-^{14}C]OA (100 or 400 µM) and accumulation over 24 h was determined with scintillation proximity assay. Accumulation was determined in presence of DMSO (0.1%) (A, B) or in presence of the adipose triglyceride lipase inhibitor (Atglistatin, 10 µM) (C, D). The results are presented as means ± SEM (n = 3, *$P < 0.05$ vs. $Plin2^{+/+}$ across all points in time). E: The effect of Atglistatin on accumulation of [1-^{14}C]OA assessed as an average of all time points from A–D. F: Cell-associated [1-^{14}C]OA after 24 h incubation with 100 µM OA in presence of the lipase inhibitor (CAY10499, 10 µM) or CAY10499 combined with Atglistatin (10 µM). For E and F, the results are presented as means ± SEM normalized to DMSO treated $Plin2^{+/+}$ myotubes (n = 3, #$P < 0.05$ vs. DMSO).

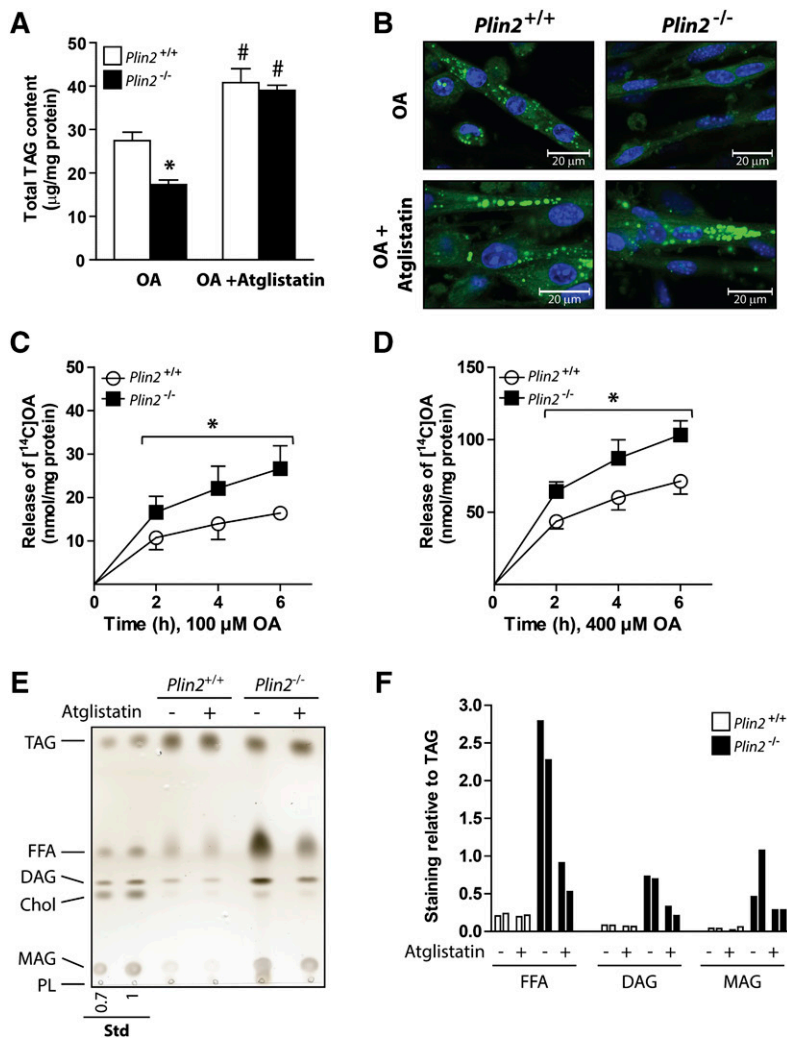**Fig. 4.** Lipolysis in OA-loaded $Plin2^{+/+}$ and $Plin2^{-/-}$ myotubes. Myotubes were incubated for 24 h with OA (100 μM) alone (0.1% DMSO) or in the presence of the adipose triglyceride lipase inhibitor Atglistatin (10 μM). A: Total triacylglycerol (TAG) content in $Plin2^{+/+}$ and $Plin2^{-/-}$ myotubes. The results are presented as means ± SEM (n = 3, *$P < 0.05$ vs. $Plin2^{+/+}$, #$P < 0.05$ vs. OA). B: Confocal pictures of $Plin2^{+/+}$ and $Plin2^{-/-}$ myotubes. Fixated myotubes were labeled with fluorescent dyes sequestering in neutral lipid droplets (Bodipy 493/503, green) or in nuclei (Hoechst 33342, blue). C, D: Lipolysis (efflux) of OA after 24 h accumulation with [1-^{14}C]OA (100 or 400 μM) in the presence of Atglistatin (10 μM). The results are presented as the release of accumulated [1-^{14}C]OA to the medium at the various time points given as means ± SEM (n = 3–7, *$P < 0.05$ vs. $Plin2^{+/+}$ across all time points). E: Cells were incubated with OA (200 μM) alone or in combination with Atglistatin (10 μM) for 24 h prior to isolation of lipid droplets and separation of lipid species with TLC. One representative of two independent experiments is shown. F: Staining intensities for the various bands in relation to the TAG signal (n = 2). Chol, cholesterol; Std, standard.

and thus incubated $Plin2^{+/+}$ and $Plin2^{-/-}$ myotubes with [1-^{14}C]OA for 24 h before CO_2 production was captured over 4 h. Although cell-associated OA was lower in $Plin2^{-/-}$ myotubes than in $Plin2^{+/+}$ myotubes (**Fig. 5A**), CO_2 produced through oxidation of the stored intracellular lipids was higher in $Plin2^{-/-}$ than in $Plin2^{+/+}$ myotubes when preincubated with 100 μM OA alone or in combination with the lipolysis inhibitor CAY10499 (Fig. 5B). Clearly, a large fraction of the produced CO_2 originated from intracellular LDs in both $Plin2^{+/+}$ and $Plin2^{-/-}$ myotubes, because CO_2 production was drastically decreased in the presence of CAY10499. Similar results for increased CO_2 production (i.e., FA oxidation) in $Plin2^{-/-}$ myotubes were obtained when cultures were preincubated with 400 μM OA (results not shown). Intermediary OA β-oxidation, measured as ASMs released from the myotubes into the cell media for 4 h, was also higher in $Plin2^{-/-}$ than in $Plin2^{+/+}$ myotubes, regardless of treatment (Fig. 5C). ASMs were similarly decreased in the two myotube populations in the presence of the lipase inhibitors CAY10499 and Atglistatin (Fig. 5C).

Absence of Plin2 in myotubes decreased both cell-associated glucose and glucose oxidation

Muscle contraction derives energy from stored glucose as glycogen and FA as TAG. Therefore, elevated FA oxidation

in the absence of $Plin2^{-/-}$ may be coordinated with altered glucose metabolism. To measure glucose oxidation, we preincubated $Plin2^{+/+}$ and $Plin2^{-/-}$ myotubes with BSA (40 μM) or OA (100 μM) for 24 h before CO_2 production from D-[^{14}C(U)]glucose was captured over 4 h. Cell-associated glucose was lower in $Plin2^{-/-}$ myotubes than in $Plin2^{+/+}$ myotubes (Fig. 5D), as was the glucose oxidation (Fig. 5E). Furthermore, preincubation with OA for 24 h suppressed glucose oxidation approximately two-fold in $Plin2^{-/-}$ myotubes in relation to $Plin2^{+/+}$ myotubes (Fig. 5E), consistent with an inverse correlation between energy derived from FA or glucose oxidation in myotubes. Collectively, these substrate oxidative assays reveal a shift in energy metabolism from utilization of glucose toward that of FAs in $Plin2^{-/-}$ myotubes.

Expression of genes involved in FA and glucose metabolism in the absence of Plin2

Prolonged changes in intracellular FA concentrations can directly affect the expression of several transcriptional factors and consequently the transcription of targeted gene families (43–45). First, we examined mRNA expression levels of *Ppar* members in $Plin2^{+/+}$ and $Plin2^{-/-}$ myotubes (**Fig. 6A**), because these transcription factors are known to be activated by various lipid moieties (46, 47). *Ppard*, the
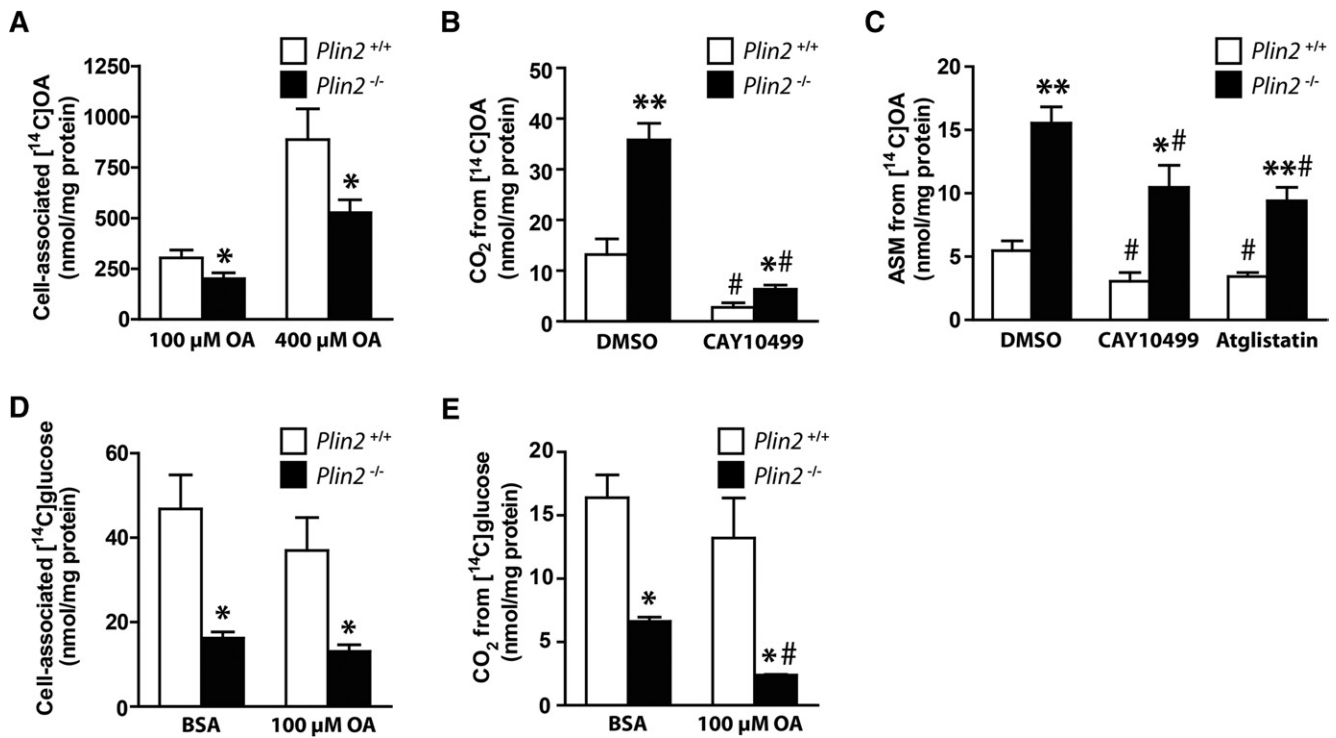
Fig. 5. Cell-associated radioactivity and oxidation of OA and glucose in $Plin2^{+/+}$ and $Plin2^{-/-}$ myotubes. For measurement of cell-associated radioactivity and oxidation of fatty acids (A–C), myotubes were preincubated with [1-^{14}C]OA (100 or 400 μM) alone (0.1% DMSO) or in the presence of CAY10499 (10 μM) or Atglistatin (10 μM) for 24 h and then subjected to FA substrate oxidation assay for 4 h. A: Total cell-associated [^{14}C]radioactivity remaining in $Plin2^{+/+}$ and $Plin2^{-/-}$ myotubes after 4 h. B: Released CO_2 arising from accumulated [^{14}C]radioactivity after 4 h. C: FA intermediary oxidation products measured as [^{14}C]radiolabeled ASMs released from the myotubes into the cell media during 24 h incubation with [^{14}C]OA. The results are presented as means ± SEM (n = 3–7, *$P < 0.05$ and **$P < 0.01$ vs. $Plin2^{+/+}$, #$P < 0.05$ vs. DMSO). For measurement of cell-associated radioactivity and oxidation of glucose (D, E), myotubes were preincubated with BSA (40 μM, i.e., basal) or OA (100 μM) for 24 h, before myotubes were incubated with D-[^{14}C(U)]glucose and subjected to glucose substrate oxidation assay for 4 h. D: Total cell-associated [^{14}C]radioactivity accumulated in myotubes after 4 h. E: Released CO_2 from oxidation of D-[^{14}C(U)]glucose. Results are presented as means ± SEM (n = 3–6, *$P < 0.05$ vs. $Plin2^{+/+}$, #$P < 0.05$ vs. BSA).

predominant subtype in skeletal muscle, was expressed to similar levels in $Plin2^{+/+}$ and $Plin2^{-/-}$ myotubes (Fig. 6A), whereas the subtypes *Ppara* and *Pparg* displayed completely opposite expression patterns (Fig. 6A). *Ppara* controls the expression of genes involved in FA oxidation (45) and was induced ∼10-fold in the $Plin2^{-/-}$ myotubes, with elevated FA levels compared with $Plin2^{+/+}$ myotubes. Conversely, *Pparg* controls the expression of genes involved in FA storage and its expression was suppressed ∼15-fold in $Plin2^{-/-}$ myotubes compared with $Plin2^{+/+}$ myotubes. Furthermore, the Ppar γ coactivator 1 α (*Ppargc1a*), a master regulator of mitochondrial biogenesis (48), was elevated ∼2-fold in $Plin2^{-/-}$ compared with $Plin2^{+/+}$ myotubes (Fig. 6A). Others have reported that mice with transgenic overexpression of *Ppara* in muscle have increased FA oxidation and reduced glucose oxidation (49) and that overexpression of *Ppargc1a* in myotubes reduces glucose oxidation (50). The metabolic switches followed by overexpression of *Ppara* and *Ppargc1a* resemble what we observed in the $Plin2^{-/-}$ myotubes that also overexpress *Ppara* and *Ppargc1a*. These results imply that a *Ppara*/*Ppargc1a* component pathway is participatory in regulating FA versus glucose oxidative balance in myotubes lacking *Plin2*. Hence, we focused our continuing analyses on the expression of genes with linkage to FA and glucose oxidative pathways, which have been

shown previously to be transcriptionally regulated by this transcription factor pathway.

Among the genes important for FA oxidation, expression of plasma membrane FA transporter CD36 antigen (*Cd36*) and mitochondrial FA transporter carnitine palmitoyltransferase 2 (*Cpt2*) mRNAs were elevated in $Plin2^{-/-}$ compared with $Plin2^{+/+}$ myotubes (Fig. 6B). Although no changes were observed for FA-binding protein 3 (*Fabp3*), higher mRNA expressions of uncoupling proteins 2 and 3 (*Ucp2* and *Ucp3*), routinely associated with elevated FA oxidation, were also observed (Fig. 6B). Collectively, the expression of mRNAs for several enzymes oxidizing acyl-CoA to acetyl-CoA, such as the mitochondrial acyl-CoA dehydrogenases (*Acadm, Acadl, Acadvl*) and peroxisomal acyl-CoA oxidase 1 (*Acox1*), were unchanged in $Plin2^{-/-}$ compared with $Plin2^{+/+}$ myotubes (Fig. 6C).

We next analyzed expression of genes involved in glucose oxidative pathways (Fig. 6D–F). Expression of solute carrier family 2 member 1 (*Slc2a1*), encoding for the basal glucose transporter 1 (Glut1), was ∼50% lower in $Plin2^{-/-}$ myotubes than in $Plin2^{+/+}$ myotubes (Fig. 6D), whereas expression of *Slc2a4*, encoding for the insulin-responsive Glut4, was unaltered (Fig. 6D). Hexokinase 1 and 2 (*Hk1* and *Hk2*), important for mobilization of glucose, and glycogen synthase 1 (*Gys1*) were also unaltered in expression (Fig. 6D).
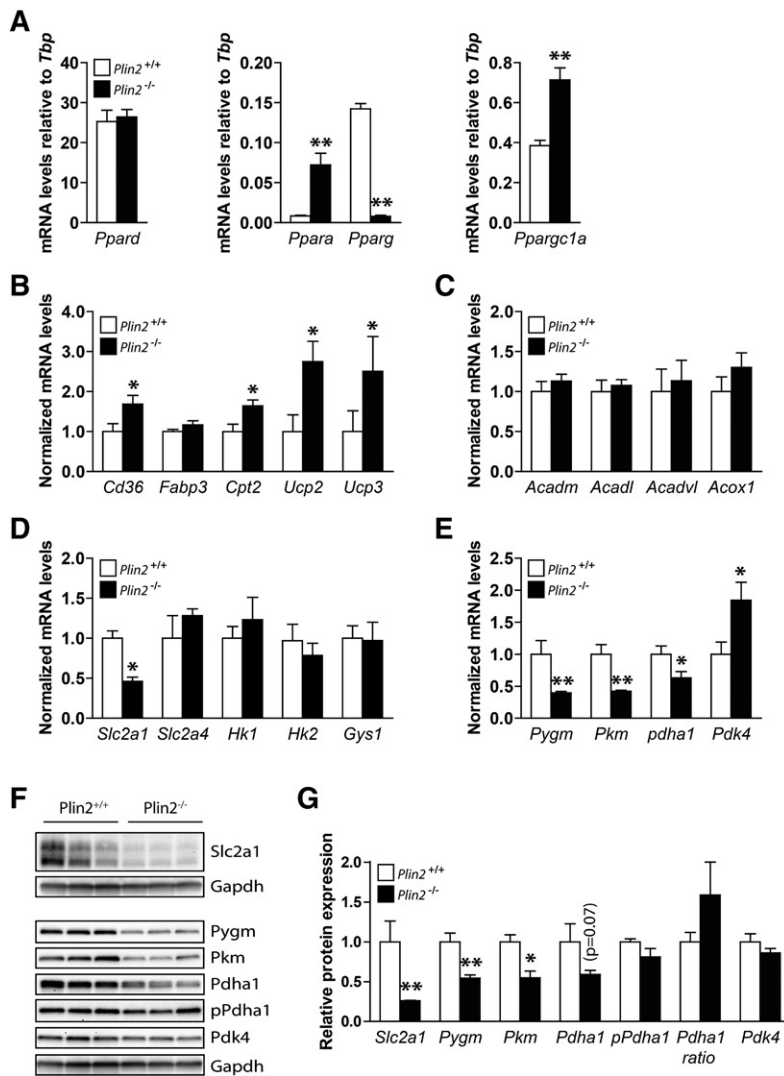
Fig. 6. Expression of genes involved in lipid metabolism in $Plin2^{+/+}$ and $Plin2^{-/-}$ myotubes. Gene expression of various mRNAs in differentiated $Plin2^{+/+}$ and $Plin2^{-/-}$ myotubes was analyzed by RT-qPCR and related to the expression of TATA-box binding protein (*Tbp*). A: Expression of transcription factors activated by FAs; Ppar α, γ and δ and Ppar γ coactivator 1 α (*Ppargc1a*). Results are presented as means ± SEM (n = 4, *$P < 0.05$ and **$P < 0.01$ vs. $Plin2^{+/+}$). B: Expression of genes involved in lipid uptake and mitochondrial function; FA transporter/CD36 antigen (*Cd36*), *Fabp3*, *Cpt2*, and uncoupling proteins 2 and 3 (*Ucp2* and *Ucp3*, respectively). C: Expression of genes catalyzing oxidation of FAs; mitochondrial *Acadm*, *Acadl*, *Acadvl*, and peroxisomal *Acox1*. D: Expression of genes involved in glucose uptake and storage; solute carrier family 2 member 1 and 4 (*Slc2a1* and *Slc2a4*, respectively), hexokinase 1 and 2 (*Hk1* and *Hk2*, respectively) and *Gys1*. E: Expression of genes involved in glycogen mobilization and glucose oxidation; muscle-associated glycogen phosphorylase(*Pygm*), muscle pyruvate kinase (*Pkm*), pyruvate dehydrogenase α 1 (*Pdha1*), and pyruvate dehydrogenase kinase 4 (*Pdk4*). Results in B–F are presented as means ± SEM normalized to the expression in $Plin2^{+/+}$ myotubes (n = 5, *$P < 0.05$, **$P < 0.01$ vs. $Plin2^{+/+}$). F: Protein content of Slc2a1, Pygm, Pkm, Pdha1, Pdha1 phosphorylated at Ser300 (pPdha1), and Pdk4 (n = 3). G: Protein content, related to Gapdh normalized to the expression levels in $Plin2^{+/+}$ myotubes, or the ratio of pPdha1 against total Pdha1 (Pdha1 ratio). The results are presented as means ± SEM (n = 3, *$P < 0.05$ vs. $Plin2^{+/+}$).

However, muscle-associated glycogen phosphorylase (*Pygm*), muscle pyruvate kinase (*Pkm*), and muscle pyruvate dehydrogenase α 1 (*Pdha1*), encoding for three enzymes that drive glucose oxidation via mobilization of pyruvate for the TCA cycle, were all less expressed in $Plin2^{-/-}$ than in $Plin2^{+/+}$ myotubes (Fig. 6E). Pyruvate dehydrogenase kinase 4 (*Pdk4*), which phosphorylates Pdha1 at Ser300 and inhibits Pdha1 enzymatic activity, was expressed at higher levels in $Plin2^{-/-}$ than in $Plin2^{+/+}$ myotubes (Fig. 6E).

We finally analyzed whether the altered gene transcript levels of the glucose transporter and the oxidative enzymes were reflected in protein level changes. Protein levels of Glut1, Pygm, Pkm, and to a lesser extent Pdha1 ($P = 0.7$), were all lower in $Plin2^{-/-}$ than in $Plin2^{+/+}$ myotubes (Fig. 6F, G), and there was a further trended ratio for elevated levels of inactive phosphorylated Pdha1 (Ser300) to total Pdha1 ($P = 0.1$) in $Plin2^{-/-}$ than in $Plin2^{+/+}$ myotubes. Taken together, the altered gene expressions in pathways for FA (*Cd36*) and glucose (*Slc2a1*) transport, glycogen degradation (*Pygm*) and glycolysis (*Pkm*, *Phda1*, and *Pdk4*) found in the $Plin2^{-/-}$ myotubes follows similar trends as for mice with muscle overexpression of *Ppara* (49) or *Ppargc1a* (50). Interestingly, all these models exhibit

metabolic biases toward FA oxidation with a corresponding suppression of glucose oxidation. This change in oxidative balance may be further supported by the feedback inhibition of glucose oxidation by accumulated acyl-CoA substrates.

Absence of Plin2 had no impact on insulin-stimulated phosphorylation of Akt

An important physiological role for skeletal muscle is whole-body glucose regulation by responding to insulin and thereby regulating active glucose transport into muscle cells. Mice with muscle-specific deletion of *Pparg* (51) or muscle-specific overexpression of *Ppara* (49) are both insulin resistant. Because $Plin2^{-/-}$ myotubes oxidized less glucose, had suppressed levels of *Pparg*, and had elevated levels of *Ppara*, we analyzed insulin response in $Plin2^{+/+}$ and $Plin2^{-/-}$ myotubes. Compared with muscle tissue in vivo, cultured myotubes respond with only a modest increase in glucose uptake after insulin stimulation (52). Despite this reduced response, cultured myotubes provide a reliable model for testing factors affecting insulin signaling. First, we compared glycogen synthesis, which indirectly reflects cellular glucose uptake, after 24 h preincubation with

either BSA (40 µM) or OA (100 µM), followed by incorporation of D-[^{14}C(U)]glucose into glycogen for 3 h. The total amount of synthesized glycogen was lower in $Plin2^{-/-}$ than in $Plin2^{+/+}$ myotubes (**Fig. 7A**) but the fold induction of glycogen synthesis by insulin stimulation was essentially the same (Fig. 7A). To further determine whether the altered FA and glucose metabolism in $Plin2^{-/-}$ myotubes affected insulin signaling, we determined insulin-stimulated mTORC2-mediated phosphorylation (Ser473) of the serine-threonine protein kinase Akt in the two cell populations. Akt phosphorylation in response to insulin was similar in $Plin2^{+/+}$ and $Plin2^{-/-}$ myotubes (Fig. 7B, C), despite total Akt (Akt1-3) being expressed at lower levels in $Plin2^{-/-}$ myotubes than in $Plin2^{+/+}$ myotubes (Fig. 7D). These findings suggest that although $Plin2^{-/-}$ myotubes have reduced basal glucose uptake compared with $Plin^{+/+}$ myotubes, insulin signaling and insulin-stimulated glucose uptake are unaffected by removal of Plin2.

DISCUSSION

Plin2 was the second Plin-family member identified as a LD surface-coating protein (53), but its function in whole-body lipid metabolism is still poorly understood. Most cell types transcribe a high pool of $Plin2$ mRNA but contain only a modest amount of the protein because of a rapid proteasomal degradation of the Plin2 pool that is not associated with LDs (31). Manipulation of $Plin2$ mRNA with temporal gene silencing (54) or overexpression of Plin2 (55) may therefore result in only modest changes in Plin2 protein levels. This phenomenon and a likely partial functional redundancy among some Plins (54) complicate studies on Plin2 function. The expression of $Plin2$ mRNA is induced and the produced Plin2 protein stabilized once LDs are formed in cells exposed to elevated levels of FAs. One example of this phenomenon is the large increase in $Plin2$ mRNA, Plin2 protein, and TAG-containing LDs in

the liver of fasted mice (56). The significance of the fasting-induced hepatic Plin2 is unclear. Characterization of two separate $Plin2$ null mouse models demonstrates that lack of $Plin2$ protects against hepatosteatosis (24, 57, 58), emphasizing that Plin2 coating of LDs may not always be beneficial. The absence of $Plin2$ also suppresses obesity in mice on certain high-caloric diets (58), despite that Plin2 protein is normally not present on adipose LDs (53), arguing that a lack of Plin2 in other tissues has an impact on energy storage and metabolism.

The consequences for muscle energy metabolism upon $Plin2$ removal had not been fully investigated previously. To shed light on the function of Plin2 in skeletal muscle, we established myoblast cultures from $Plin2^{+/+}$ and $Plin2^{-/-}$ mice. Given the known discrepancies in Plin2 mRNA and protein levels, our system with an absence of functional $Plin2$ differs from earlier studies based on siRNA knockdown or ectopic expression of Plin2 (54, 55). In a manner similar to that in the earlier studies based on the partial depletion of Plin2 (54, 55), we show in this study that myotubes that lack $Plin2$ have less accumulated TAG than wild-type myotubes. When $Plin2^{-/-}$ myotubes were exposed to Atglistatin, an inhibitor of ATGL that reduces lipolysis of TAG in LDs, TAG content was comparable to $Plin2^{+/+}$ myotubes, whereas removal of the inhibitor resulted in a faster release of FAs from the accumulated TAG pool in $Plin2^{-/-}$ myotubes. The LDs retained in $Plin2^{-/-}$ myotubes furthermore consist of reduced amount of TAG in relation to a higher amount of lipolytic degradation products such as DAG, MAG, and FFA compared with $Plin2^{+/+}$ myotubes. These results suggest that a lack of Plin2 on LDs does not affect FA uptake or incorporation into LDs per se, but its absence increases degradation of the TAG deposited within LDs through enhanced lipolysis. Our observations complement other studies, suggesting that overexpression of Plin2 in embryonic kidney cells reduced the interaction of lipases with LDs (59) or that a combined $Plin2$ and $Plin3$ knockdown increased lipolysis in hepatocytes (54). Consistent with a model in which reduced TAG in
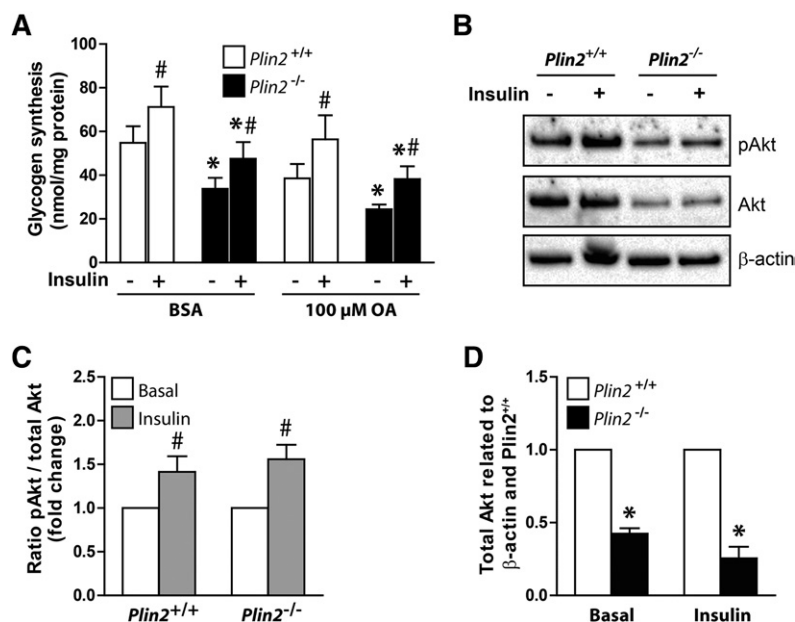

Fig. 7. Effect of insulin in $Plin2^{+/+}$ and $Plin2^{-/-}$ myotubes. A: Myotubes were preincubated with BSA (40 µM) or OA (100 µM) for 24 h. Glycogen synthesis was subsequently measured as incorporation of D-[^{14}C(U)]glucose into glycogen in the absence or presence of insulin (100 nM) for 3 h. B: Myotubes were preincubated with OA (100 µM) for 24 h, then incubated in glucose-free medium supplemented with OA (100 µM) for 2 h, and subsequently incubated in medium containing glucose (5.5 mM) with or without insulin (100 nM) for 15 min. Cell samples were subjected for immunoblotting analysis with antibodies against total Akt (Akt1-3), pAkt (Ser473), and β-actin (housekeeping protein). Immunoblots from one representative experiment are shown. C: Ratio of pAkt/total Akt related to myotubes receiving no insulin. D: The content of total Akt related to β-actin normalized to expression levels in $Plin2^{+/+}$ myotubes. The results are presented as means ± SEM (n = 4, *$P < 0.05$ vs. $Plin2^{+/+}$ with the same treatment, #$P < 0.05$ vs. without insulin). pAkt, phosphorylated Akt.

$Plin2^{-/-}$ myotubes is caused by elevated lipolytic activity, skeletal muscles of ATGL null mice show increased TAG accumulation and reduced lipolysis (60). In our study, inhibitors of ATGL (i.e., Atglistatin) or ATGL and HSL (i.e. CAY10499) enhanced LD content and elevated total accumulated TAG with considerably higher potency in $Plin2^{-/-}$ myotubes than in $Plin2^{+/+}$ myotubes. These results support the notion that ATGL and HSL have limited access to LDs or have reduced activity in myotubes expressing Plin2 at the LD surface. Taken together, our results establish that one functional role for Plin2 in muscle is to protect TAG stored within LDs from lipases such as ATGL or HSL.

Metabolic consequences upon *Plin2* removal may at least partly be caused by increased efflux of FAs from LDs in $Plin2^{-/-}$ myotubes. We observed a profound increase in OA oxidation and a reduction in glucose oxidation in $Plin2^{-/-}$ myotubes. In line with a functional role of Plin2 as a protector of TAG stored within LDs, we observed that $Plin2^{-/-}$ myotubes exposed to OA accumulated less DAG. Previous experiments in myotubes depleted of *Plin2* by siRNA showed a more modest increase in palmitic acid (PA) oxidation but also an increase in DAG (55). The incomplete removal of the Plin2 protein in *Plin2* siRNA knockdown myotubes compared with an absence of Plin2 in our $Plin2^{-/-}$ myotubes likely contributes to these discrepancies. The different types of labeled FAs used may also be significant. PA is accumulated to a lower extent into LDs than is OA in myotubes (61). The strong repression of FA oxidation observed in myotubes exposed to the dual ATGL and HSL lipase inhibitor (CAY10499) demonstrates that OA converted into CO_2 derived mainly from LDs in our experiments. Consistent with LDs being an important source of substrate for FA oxidation, other investigators have reported that preservation of LDs by knockdown of the ATGL coactivator CGI-58 decreased lipolysis and FA oxidation while increasing glucose oxidation and incorporation into glycogen in cultured myotubes (62).

The enhanced release of FAs from the LDs observed in $Plin2^{-/-}$ myotubes may support inhibition of glucose oxidation and stimulation of FA oxidation via mutual inhibition of substrate metabolism in the glucose-FA cycle (43). A similar enhanced FA oxidation is found in cultured hepatocytes isolated from $Plin2^{-/-}$ mice (Y.K.L., K.T.D., and A.R.K., unpublished observations). Our data define a mechanistic function for Plin2 to regulate TAG stores and FA oxidation, in an antagonistic pathway that balances glucose oxidation. The observed alterations in expressions of genes facilitating glucose uptake and oxidation are consistent with the glucose-FA cycle described by Randle, which defines a metabolic competition between glucose and FAs, in which enhanced FA availability suppresses glucose oxidation. We observed decreased levels of proteins involved both in glucose uptake (Slc2a1/Glut1) and in glucose oxidation in $Plin2^{-/-}$ myotubes, consistent with studies examining how elevated circulating FAs inhibit glucose oxidation in human skeletal muscle (63). To facilitate such an energy substrate switch, transcription factors known to stimulate expression of genes driving FA oxidation such as *Ppara* and *Ppargc1a* (64) were expressed at higher levels in $Plin2^{-/-}$ myotubes, whereas *Pparg*, which stimulates expression of genes promoting lipid storage (65),

were suppressed. Elevated expression of *Ppara* has previously been noted in livers of $Plin2^{-/-}$ mice (58), consistent with an opposite repression of *Ppara* expression in muscle overexpressing Plin2 (55). Interestingly, we found that our cultured $Plin2^{-/-}$ myotubes resemble the FA oxidative phenotype and repressed expression of glucose oxidative genes characteristic of muscle cells that were engineered to overexpress either *Ppara* (49) or *Ppargc1a* (50). We also observed enhanced expression of uncoupling proteins, which disconnects energy production from oxidative flux when FA levels are too elevated. Taken together, our data suggest an increased acyl-CoA to acetyl-CoA flux in $Plin2^{-/-}$ myotubes, as modeled in the Randle cycle, serving to metabolically inhibit and suppress expression of glycolytic enzymes and reduce glucose oxidation and favor FA oxidation.

With respect to insulin responsiveness, Plin2 loss-of-function studies in liver or whole animals have shown contradictory results (54, 57, 66, 67). In our study, $Plin2^{+/+}$ and $Plin2^{-/-}$ myotubes had comparable insulin-stimulated responses judged by the increase in total Akt phosphorylation and glycogen synthesis, whereas glucose accumulation and oxidation were markedly decreased in $Plin2^{-/-}$ myotubes. Normal insulin signaling was also reported after *Plin2* knockdown in C2C12 myotubes (55). It has been proposed that accumulation of lipotoxic intermediates in cells exposed to high levels of FAs may interfere with insulin signaling because of a mismatch among lipid storage, lipolysis, and oxidation (68). Enhanced FA oxidation in $Plin2^{-/-}$ myotubes may therefore act as a compensatory mechanism to handle the increased availability of FAs released from the more rapidly degrading LDs. It remains to be investigated further whether the reduced expressions of Akt proteins, measured with a pan-Akt antibody, mechanistically contribute to reduced glucose metabolism in $Plin2^{-/-}$ myotubes. The three different Akt isoforms (Akt1-3) have distinct roles, in which Akt2 is particularly involved in the maintenance of glucose homeostasis (69). Further studies are required to clarify whether a particular Akt protein is reduced in $Plin2^{-/-}$ myotubes and signals to reduce glucose uptake.

In summary, by characterizing myotubes established from $Plin2^{+/+}$ and $Plin2^{-/-}$ mice, we demonstrate that loss of *Plin2* results in myotubes with reduced accumulation of neutral lipids in LDs due to elevated lipolysis. Similar to what has been shown previously for Plin1 and Plin5 (21, 70), this establishes a functional role of Plin2 as a protector against lipolytic degradation of LDs. The increased efflux of FAs from LDs in $Plin2^{-/-}$ myotubes is likely to contribute to a metabolic shift in energy metabolism from utilization of glucose toward FAs. Such a shift may be facilitated by altered transcription of metabolic regulators in $Plin2^{-/-}$ myotubes. Our results demonstrate that Plin2 is essential for balancing the pool of LDs in cultured myotubes to avoid an uncontrolled hydrolysis of intracellular TAG and altered energy metabolism caused by increased release of FAs from LDs.⬛

REFERENCES

1. Hue, L., and H. Taegtmeyer. 2009. The Randle cycle revisited: a new head for an old hat. *Am. J. Physiol. Endocrinol. Metab.* **297:** E578–E591.

2. Eckardt, K., A. Taube, and J. Eckel. 2011. Obesity-associated insulin resistance in skeletal muscle: role of lipid accumulation and physical inactivity. *Rev. Endocr. Metab. Disord.* **12:** 163–172.

3. Samuel, V. T., and G. I. Shulman. 2012. Mechanisms for insulin resistance: common threads and missing links. *Cell.* **148:** 852–871.

4. Pan, D. A., S. Lillioja, A. D. Kriketos, M. R. Milner, L. A. Baur, C. Bogardus, A. B. Jenkins, and L. H. Storlien. 1997. Skeletal muscle triglyceride levels are inversely related to insulin action. *Diabetes.* **46:** 983–988.

5. Jacob, S., J. Machann, K. Rett, K. Brechtel, A. Volk, W. Renn, E. Maerker, S. Matthaei, F. Schick, C. D. Claussen, et al. 1999. Association of increased intramyocellular lipid content with insulin resistance in lean nondiabetic offspring of type 2 diabetic subjects. *Diabetes.* **48:** 1113–1119.

6. Goodpaster, B. H., R. Theriault, S. C. Watkins, and D. E. Kelley. 2000. Intramuscular lipid content is increased in obesity and decreased by weight loss. *Metabolism.* **49:** 467–472.

7. van Loon, L. J., R. Koopman, R. Manders, W. van der Weegen, G. P. van Kranenburg, and H. A. Keizer. 2004. Intramyocellular lipid content in type 2 diabetes patients compared with overweight sedentary men and highly trained endurance athletes. *Am. J. Physiol. Endocrinol. Metab.* **287:** E558–E565.

8. Sztalryd, C., and A. R. Kimmel. 2014. Perilipins: lipid droplet coat proteins adapted for tissue-specific energy storage and utilization, and lipid cytoprotection. *Biochimie.* **96:** 96–101.

9. Goodpaster, B. H., J. He, S. Watkins, and D. E. Kelley. 2001. Skeletal muscle lipid content and insulin resistance: evidence for a paradox in endurance-trained athletes. *J. Clin. Endocrinol. Metab.* **86:** 5755–5761.

10. Amati, F., J. J. Dube, E. Alvarez-Carnero, M. M. Edreira, P. Chomentowski, P. M. Coen, G. E. Switzer, P. E. Bickel, M. Stefanovic-Racic, F. G. Toledo, et al. 2011. Skeletal muscle triglycerides, diacylglycerols, and ceramides in insulin resistance: another paradox in endurance-trained athletes? *Diabetes.* **60:** 2588–2597.

11. Høeg, L., C. Roepstorff, M. Thiele, E. A. Richter, J. F. Wojtaszewski, and B. Kiens. 2009. Higher intramuscular triacylglycerol in women does not impair insulin sensitivity and proximal insulin signaling. *J. Appl. Physiol.* **107:** 824–831.

12. Coen, P. M., and B. H. Goodpaster. 2012. Role of intramyocelluar lipids in human health. *Trends Endocrinol. Metab.* **23:** 391–398.

13. Brasaemle, D. L. 2007. Thematic review series: adipocyte biology. The perilipin family of structural lipid droplet proteins: stabilization of lipid droplets and control of lipolysis. *J. Lipid Res.* **48:** 2547–2559.

14. Bickel, P. E., J. T. Tansey, and M. A. Welte. 2009. PAT proteins, an ancient family of lipid droplet proteins that regulate cellular lipid stores. *Biochim. Biophys. Acta.* **1791:** 419–440.

15. Zimmermann, R., J. G. Strauss, G. Haemmerle, G. Schoiswohl, R. Birner-Gruenberger, M. Riederer, A. Lass, G. Neuberger, F. Eisenhaber, A. Hermetter, et al. 2004. Fat mobilization in adipose tissue is promoted by adipose triglyceride lipase. *Science.* **306:** 1383–1386.

16. Haemmerle, G., R. Zimmermann, M. Hayn, C. Theussl, G. Waeg, E. Wagner, W. Sattler, T. M. Magin, E. F. Wagner, and R. Zechner. 2002. Hormone-sensitive lipase deficiency in mice causes diglyceride accumulation in adipose tissue, muscle, and testis. *J. Biol. Chem.* **277:** 4806–4815.

17. Fredrikson, G., H. Tornqvist, and P. Belfrage. 1986. Hormone-sensitive lipase and monoacylglycerol lipase are both required for complete degradation of adipocyte triacylglycerol. *Biochim. Biophys. Acta.* **876:** 288–293.

18. Kimmel, A. R., and C. Sztalryd. 2016. The perilipins: major cytosolic lipid droplet-associated proteins and their roles in cellular lipid storage, mobilization, and systemic homeostasis. *Annu. Rev. Nutr.* **36:** 471–509.

19. Kimmel, A. R., D. L. Brasaemle, M. McAndrews-Hill, C. Sztalryd, and C. Londos. 2010. Adoption of PERILIPIN as a unifying nomenclature for the mammalian PAT-family of intracellular lipid storage droplet proteins. *J. Lipid Res.* **51:** 468–471.

20. Dalen, K. T., T. Dahl, E. Holter, B. Arntsen, C. Londos, C. Sztalryd, and H. I. Nebb. 2007. LSDP5 is a PAT protein specifically expressed in fatty acid oxidizing tissues. *Biochim. Biophys. Acta.* **1771:** 210–227.

21. Sztalryd, C., G. Xu, H. Dorward, J. T. Tansey, J. A. Contreras, A. R. Kimmel, and C. Londos. 2003. Perilipin A is essential for the translocation of hormone-sensitive lipase during lipolytic activation. *J. Cell Biol.* **161:** 1093–1103.

22. Martinez-Botas, J., J. B. Anderson, D. Tessier, A. Lapillonne, B. H. Chang, M. J. Quast, D. Gorenstein, K. H. Chen, and L. Chan. 2000. Absence of perilipin results in leanness and reverses obesity in Lepr(db/db) mice. *Nat. Genet.* **26:** 474–479.

23. Tansey, J. T., C. Sztalryd, J. Gruia-Gray, D. L. Roush, J. V. Zee, O. Gavrilova, M. L. Reitman, C. X. Deng, C. Li, A. R. Kimmel, et al. 2001. Perilipin ablation results in a lean mouse with aberrant adipocyte lipolysis, enhanced leptin production, and resistance to diet-induced obesity. *Proc. Natl. Acad. Sci. USA.* **98:** 6494–6499.

24. Chang, B. H., L. Li, A. Paul, S. Taniguchi, V. Nannegari, W. C. Heird, and L. Chan. 2006. Protection against fatty liver but normal adipogenesis in mice lacking adipose differentiation-related protein. *Mol. Cell. Biol.* **26:** 1063–1076.

25. Chen, W., B. Chang, X. Wu, L. Li, M. Sleeman, and L. Chan. 2013. Inactivation of Plin4 downregulates Plin5 and reduces cardiac lipid accumulation in mice. *Am. J. Physiol. Endocrinol. Metab.* **304:** E770–E779.

26. Kuramoto, K., T. Okamura, T. Yamaguchi, T. Y. Nakamura, S. Wakabayashi, H. Morinaga, M. Nomura, T. Yanase, K. Otsu, N. Usuda, et al. 2012. Perilipin 5, a lipid droplet-binding protein, protects heart from oxidative burden by sequestering fatty acid from excessive oxidation. *J. Biol. Chem.* **287:** 23852–23863.

27. Hsieh, K., Y. K. Lee, C. Londos, B. M. Raaka, K. T. Dalen, and A. R. Kimmel. 2012. Perilipin family members preferentially sequester to either triacylglycerol-specific or cholesteryl-ester-specific intracellular lipid storage droplets. *J. Cell Sci.* **125:** 4067–4076.

28. Shaw, C. S., M. Sherlock, P. M. Stewart, and A. J. Wagenmakers. 2009. Adipophilin distribution and colocalization with lipid droplets in skeletal muscle. *Histochem. Cell Biol.* **131:** 575–581.

29. Phillips, S. A., C. C. Choe, T. P. Ciaraldi, A. S. Greenberg, A. P. Kong, S. C. Baxi, L. Christiansen, S. R. Mudaliar, and R. R. Henry. 2005. Adipocyte differentiation-related protein in human skeletal muscle: relationship to insulin sensitivity. *Obes. Res.* **13:** 1321–1329.

30. Minnaard, R., P. Schrauwen, G. Schaart, J. A. Jorgensen, E. Lenaers, M. Mensink, and M. K. Hesselink. 2009. Adipocyte differentiation-related protein and OXPAT in rat and human skeletal muscle: involvement in lipid accumulation and type 2 diabetes mellitus. *J. Clin. Endocrinol. Metab.* **94:** 4077–4085.

31. Xu, G., C. Sztalryd, X. Lu, J. T. Tansey, J. Gan, H. Dorward, A. R. Kimmel, and C. Londos. 2005. Post-translational regulation of adipose differentiation-related protein by the ubiquitin/proteasome pathway. *J. Biol. Chem.* **280:** 42841–42847.

32. Hessvik, N. P., M. V. Boekschoten, M. A. Baltzersen, S. Kersten, X. Xu, H. Andersen, A. C. Rustan, and G. H. Thoresen. 2010. LXR{beta} is the dominant LXR subtype in skeletal muscle regulating lipogenesis and cholesterol efflux. *Am. J. Physiol. Endocrinol. Metab.* **298:** E602–E613.

33. Bindesbøll, C., O. Berg, B. Arntsen, H. I. Nebb, and K. T. Dalen. 2013. Fatty acids regulate perilipin5 in muscle by activating PPARδ. *J. Lipid Res.* **54:** 1949–1963.

34. Miura, S., J. W. Gan, J. Brzostowski, M. J. Parisi, C. J. Schultz, C. Londos, B. Oliver, and A. R. Kimmel. 2002. Functional conservation for lipid storage droplet association among Perilipin, ADRP, and TIP47 (PAT)-related proteins in mammals, Drosophila, and Dictyostelium. *J. Biol. Chem.* **277:** 32253–32257.

35. Ye, J., G. Coulouris, I. Zaretskaya, I. Cutcutache, S. Rozen, and T. L. Madden. 2012. Primer-BLAST: a tool to design target-specific primers for polymerase chain reaction. *BMC Bioinformatics.* **13:** 134.

36. Hessvik, N. P., S. S. Bakke, K. Fredriksson, M. V. Boekschoten, A. Fjorkenstad, G. Koster, M. K. Hesselink, S. Kersten, E. T. Kase, A. C. Rustan, et al. 2010. Metabolic switching of human myotubes is improved by n-3 fatty acids. *J. Lipid Res.* **51:** 2090–2104.

37. Wensaas, A. J., A. C. Rustan, K. Lovstedt, B. Kull, S. Wikstrom, C. A. Drevon, and S. Hallen. 2007. Cell-based multiwell assays for the detection of substrate accumulation and oxidation. *J. Lipid Res.* **48:** 961–967.

38. Mayer, N., M. Schweiger, M. Romauch, G. F. Grabner, T. O. Eichmann, E. Fuchs, J. Ivkovic, C. Heier, I. Mrak, A. Lass, et al. 2013.

Development of small-molecule inhibitors targeting adipose triglyceride lipase. *Nat. Chem. Biol.* **9:** 785–787.

39. Weerheim, A. M., A. M. Kolb, A. Sturk, and R. Nieuwland. 2002. Phospholipid composition of cell-derived microparticles determined by one-dimensional high-performance thin-layer chromatography. *Anal. Biochem.* **302:** 191–198.

40. Gaster, M., A. C. Rustan, V. Aas, and H. Beck-Nielsen. 2004. Reduced lipid oxidation in skeletal muscle from type 2 diabetic subjects may be of genetic origin: evidence from cultured myotubes. *Diabetes.* **53:** 542–548.

41. Grisouard, J., E. Bouillet, K. Timper, T. Radimerski, K. Dembinski, D. M. Frey, R. Peterli, H. Zulewski, U. Keller, B. Muller, et al. 2012. Both inflammatory and classical lipolytic pathways are involved in lipopolysaccharide-induced lipolysis in human adipocytes. *Innate Immun.* **18:** 25–34.

42. Iglesias, J., J. Lamontagne, H. Erb, S. Gezzar, S. Zhao, E. Joly, V. L. Truong, K. Skorey, S. Crane, S. R. Madiraju, et al. 2016. Simplified assays of lipolysis enzymes for drug discovery and specificity assessment of known inhibitors. *J. Lipid Res.* **57:** 131–141.

43. Randle, P. J., P. B. Garland, C. N. Hales, and E. A. Newsholme. 1963. The glucose fatty-acid cycle. Its role in insulin sensitivity and the metabolic disturbances of diabetes mellitus. *Lancet.* **1:** 785–789.

44. Jump, D. B. 2004. Fatty acid regulation of gene transcription. *Crit. Rev. Clin. Lab. Sci.* **41:** 41–78.

45. Georgiadi, A., and S. Kersten. 2012. Mechanisms of gene regulation by fatty acids. *Adv. Nutr.* **3:** 127–134.

46. Poulsen, L., M. Siersbaek, and S. Mandrup. 2012. PPARs: fatty acid sensors controlling metabolism. *Semin. Cell Dev. Biol.* **23:** 631–639.

47. Nakamura, M. T., B. E. Yudell, and J. J. Loor. 2014. Regulation of energy metabolism by long-chain fatty acids. *Prog. Lipid Res.* **53:** 124–144.

48. Lin, J., H. Wu, P. T. Tarr, C. Y. Zhang, Z. Wu, O. Boss, L. F. Michael, P. Puigserver, E. Isotani, E. N. Olson, et al. 2002. Transcriptional co-activator PGC-1 alpha drives the formation of slow-twitch muscle fibres. *Nature.* **418:** 797–801.

49. Finck, B. N., C. Bernal-Mizrachi, D. H. Han, T. Coleman, N. Sambandam, L. L. LaRiviere, J. O. Holloszy, C. F. Semenkovich, and D. P. Kelly. 2005. A potential link between muscle peroxisome proliferator- activated receptor-alpha signaling and obesity-related diabetes. *Cell Metab.* **1:** 133–144.

50. Wende, A. R., J. M. Huss, P. J. Schaeffer, V. Giguere, and D. P. Kelly. 2005. PGC-1alpha coactivates PDK4 gene expression via the orphan nuclear receptor ERRalpha: a mechanism for transcriptional control of muscle glucose metabolism. *Mol. Cell. Biol.* **25:** 10684–10694.

51. Hevener, A. L., W. He, Y. Barak, J. Le, G. Bandyopadhyay, P. Olson, J. Wilkes, R. M. Evans, and J. Olefsky. 2003. Muscle-specific Pparg deletion causes insulin resistance. *Nat. Med.* **9:** 1491–1497.

52. Sarabia, V., L. Lam, E. Burdett, L. A. Leiter, and A. Klip. 1992. Glucose transport in human skeletal muscle cells in culture. Stimulation by insulin and metformin. *J. Clin. Invest.* **90:** 1386–1395.

53. Brasaemle, D. L., T. Barber, N. E. Wolins, G. Serrero, E. J. Blanchette-Mackie, and C. Londos. 1997. Adipose differentiation-related protein is an ubiquitously expressed lipid storage droplet-associated protein. *J. Lipid Res.* **38:** 2249–2263.

54. Bell, M., H. Wang, H. Chen, J. C. McLenithan, D. W. Gong, R. Z. Yang, D. Yu, S. K. Fried, M. J. Quon, C. Londos, et al. 2008. Consequences of lipid droplet coat protein downregulation in liver cells: abnormal lipid droplet metabolism and induction of insulin resistance. *Diabetes.* **57:** 2037–2045.

55. Bosma, M., M. K. Hesselink, L. M. Sparks, S. Timmers, M. J. Ferraz, F. Mattijssen, D. van Beurden, G. Schaart, M. H. de Baets, F. K. Verheyen, et al. 2012. Perilipin 2 improves insulin sensitivity in skeletal muscle despite elevated intramuscular lipid levels. *Diabetes.* **61:** 2679–2690.

56. Dalen, K. T., S. M. Ulven, B. M. Arntsen, K. Solaas, and H. I. Nebb. 2006. PPARalpha activators and fasting induce the expression of adipose differentiation-related protein in liver. *J. Lipid Res.* **47:** 931–943.

57. Chang, B. H., L. Li, P. Saha, and L. Chan. 2010. Absence of adipose differentiation related protein upregulates hepatic VLDL secretion, relieves hepatosteatosis, and improves whole body insulin resistance in leptin-deficient mice. *J. Lipid Res.* **51:** 2132–2142.

58. McManaman, J. L., E. S. Bales, D. J. Orlicky, M. Jackman, P. S. MacLean, S. Cain, A. E. Crunk, A. Mansur, C. E. Graham, T. A. Bowman, et al. 2013. Perilipin-2-null mice are protected against diet-induced obesity, adipose inflammation, and fatty liver disease. *J. Lipid Res.* **54:** 1346–1359.

59. Listenberger, L. L., A. G. Ostermeyer-Fay, E. B. Goldberg, W. J. Brown, and D. A. Brown. 2007. Adipocyte differentiation-related protein reduces the lipid droplet association of adipose triglyceride lipase and slows triacylglycerol turnover. *J. Lipid Res.* **48:** 2751–2761.

60. Haemmerle, G., A. Lass, R. Zimmermann, G. Gorkiewicz, C. Meyer, J. Rozman, G. Heldmaier, R. Maier, C. Theussl, S. Eder, et al. 2006. Defective lipolysis and altered energy metabolism in mice lacking adipose triglyceride lipase. *Science.* **312:** 734–737.

61. Bakke, S. S., C. Moro, N. Nikolic, N. P. Hessvik, P. M. Badin, L. Lauvhaug, K. Fredriksson, M. K. Hesselink, M. V. Boekschoten, S. Kersten, et al. 2012. Palmitic acid follows a different metabolic pathway than oleic acid in human skeletal muscle cells; lower lipolysis rate despite an increased level of adipose triglyceride lipase. *Biochim. Biophys. Acta.* **1821:** 1323–1333.

62. Badin, P. M., C. Loubiere, M. Coonen, K. Louche, G. Tavernier, V. Bourlier, A. Mairal, A. C. Rustan, S. R. Smith, D. Langin, et al. 2012. Regulation of skeletal muscle lipolysis and oxidative metabolism by the co-lipase CGI-58. *J. Lipid Res.* **53:** 839–848.

63. Roden, M., T. B. Price, G. Perseghin, K. F. Petersen, D. L. Rothman, G. W. Cline, and G. I. Shulman. 1996. Mechanism of free fatty acid-induced insulin resistance in humans. *J. Clin. Invest.* **97:** 2859–2865.

64. Nikolić, N., M. Rhedin, A. C. Rustan, L. Storlien, G. H. Thoresen, and M. Strömstedt. 2012. Overexpression of PGC-1α increases fatty acid oxidative capacity of human skeletal muscle cells. *Biochem. Res. Int.* **2012:** 714074.

65. Azhar, S. 2010. Peroxisome proliferator-activated receptors, metabolic syndrome and cardiovascular disease. *Future Cardiol.* **6:** 657–691.

66. Imai, Y., G. M. Varela, M. B. Jackson, M. J. Graham, R. M. Crooke, and R. S. Ahima. 2007. Reduction of hepatosteatosis and lipid levels by an adipose differentiation-related protein antisense oligonucleotide. *Gastroenterology.* **132:** 1947–1954.

67. Varela, G. M., D. A. Antwi, R. Dhir, X. Yin, N. S. Singhal, M. J. Graham, R. M. Crooke, and R. S. Ahima. 2008. Inhibition of ADRP prevents diet-induced insulin resistance. *Am. J. Physiol. Gastrointest. Liver Physiol.* **295:** G621–G628.

68. Moro, C., S. Bajpeyi, and S. R. Smith. 2008. Determinants of intramyocellular triglyceride turnover: implications for insulin sensitivity. *Am. J. Physiol. Endocrinol. Metab.* **294:** E203–E213.

69. Cho, H., J. Mu, J. K. Kim, J. L. Thorvaldsen, Q. Chu, E. B. Crenshaw III, K. H. Kaestner, M. S. Bartolomei, G. I. Shulman, and M. J. Birnbaum. 2001. Insulin resistance and a diabetes mellitus-like syndrome in mice lacking the protein kinase Akt2 (PKB beta). *Science.* **292:** 1728–1731.

70. Pollak, N. M., D. Jaeger, S. Kolleritsch, R. Zimmermann, R. Zechner, A. Lass, and G. Haemmerle. 2015. The interplay of protein kinase A and perilipin 5 regulates cardiac lipolysis. *J. Biol. Chem.* **290:** 1295–1306.